

2015

Apoptosis and Cell Cycle Regulation as Mechanisms of Compensation from Notch Signaling Perturbation in the Developing Nervous System of *Xenopus laevis*

Catherine Hope Bianchi
College of William & Mary - Arts & Sciences

Follow this and additional works at: <https://scholarworks.wm.edu/etd>



Part of the [Cell Biology Commons](#)

Recommended Citation

Bianchi, Catherine Hope, "Apoptosis and Cell Cycle Regulation as Mechanisms of Compensation from Notch Signaling Perturbation in the Developing Nervous System of *Xenopus laevis*" (2015). *Dissertations, Theses, and Masters Projects*. William & Mary. Paper 1539626791.
<https://dx.doi.org/doi:10.21220/s2-mhan-gm13>

This Thesis is brought to you for free and open access by the Theses, Dissertations, & Master Projects at W&M ScholarWorks. It has been accepted for inclusion in Dissertations, Theses, and Masters Projects by an authorized administrator of W&M ScholarWorks. For more information, please contact scholarworks@wm.edu.

Apoptosis and Cell Cycle Regulation as
Mechanisms of Compensation from Notch Signaling Perturbation in the
Developing Nervous System of *Xenopus laevis*

Catherine Hope Bianchi

Rockville, Maryland

Bachelor of Science, University of Maryland-College Park, 2013

A Thesis presented to the Graduate Faculty
of the College of William and Mary in Candidacy for the Degree of
Master of Science

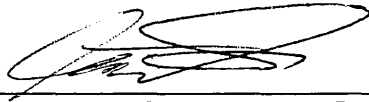
Department of Biology

The College of William and Mary
August, 2015

APPROVAL PAGE

This Thesis is submitted in partial fulfillment of
the requirements for the degree of

Master of Science



Catherine Hope Bianchi

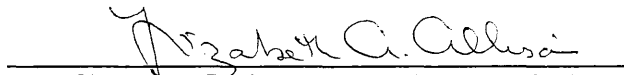
Approved by the Committee, July, 2015



Committee Chair
Chancellor Professor Margaret Saha, Biology
The College of William and Mary



Professor Diane Shakes, Biology
The College of William and Mary



Chancellor Professor Lizabeth Allison, Biology
The College of William and Mary

COMPLIANCE PAGE

Research approved by

Institutional Animal Care and Use Committee

Institutional Biohazard Committee

Protocol number(s): IACUC-2013-05-23-8750

IBC-2013-02-20-8490

Date(s) of approval: 06-01-2015

2015-03-01

ABSTRACT

The successful development of a functional nervous system hinges on the embryonic capacity to execute genetic programs in the face of developmental disturbance. Here we investigate the mechanisms of cell type recovery following the disturbance of a major juxtacrine signaling pathway in *Xenopus laevis*. During neurogenesis, neuronal differentiation is limited through lateral fate inhibition enacted by the Notch signaling pathway. We observed that early misregulation of Notch signaling leads to neural patterning defects that appear to correct over time. We hypothesized that apoptosis and cell cycle regulation are mechanisms to restore balance in neural cell populations as development progresses. The numbers of proliferating and dying neural cells as well as the expression of apoptosis pathway genes were compared over time between the control and perturbed sides of embryos with unilaterally hyperactivated or suppressed Notch signaling. Results indicate that altered cell type distribution resulting from early Notch perturbation is reflected in the total number of cells within the central nervous system, and that cell number is significantly restored by late tadpole stages. Altered levels of proliferation and apoptosis within injected neural tissue appear to contribute to this normalization in embryos with upregulated Notch signaling. We hypothesize that the death and proliferation of neural progenitor cells are differentially regulated in this condition, while the regulation of neuronal differentiation rate is involved in the recovery from signal attenuation.

TABLE OF CONTENTS

Acknowledgements	ii
List of Tables	iii
List of Figures	iv
Chapter 1. Overview of the Problem	1
Chapter 2. Review of the Literature	4
Chapter 3. Experimental Overview and Hypotheses	19
Chapter 4. Materials and Methods	22
Chapter 5. Results	35
Chapter 6. Discussion	59
Appendix	68
Bibliography	73

ACKNOWLEDGEMENTS

I would like to express my appreciation to my committee chair, Dr. Saha, who has supported me throughout my thesis and whose encouragement and feedback has guided me along the way. Her passion for science and teaching has been an inspiration throughout my time at the College, and her mentorship has been an invaluable part of my experience here.

I also extend my sincerest thanks to committee members Dr. Shakes and Dr. Allison for their advice, support, and careful criticism over the course of my thesis.

I also give my endless thanks to my wonderful mother Carole for her unending love and support at every turn.

To Claire Tocheny and Ryan Huyck I give my thanks for their great work on this project as well as their support and advice during the course of experiments and analysis.

Lastly I would like to express my appreciation for Eri Anastas, Claire Tocheny, Ryan Huyck, Mariah McKevitt, Cheyenne Williams, and other Saha lab members for their friendship, support, and guidance throughout my program.

LIST OF TABLES

1. Predicted Notch perturbation phenotypes and compensatory responses	21
2. Constructs for capped RNA and RNA probe synthesis	34
3. Neural Cell Counts for GFP-injected embryos	37
4. Neural Cell Counts for ICD-injected embryos	38
5. Neural Cell Counts for DBM-injected embryos	39
6. PCNA Cell Counts for Vehicle-Injected Controls	43
7. PCNA Cell Counts for ICD-injected embryos	44
8. PCNA Cell Counts for DBM-injected embryos	45
9. TUNEL Cell Counts for GFP-injected embryos	48
10. TUNEL Cell Counts for ICD-injected embryos	49
11. TUNEL Cell Counts for DBM-injected embryos	50
12. Expression of candidate genes assayed by in situ hybridization in control embryos	53
13. Apoptosis candidate gene functions and major modes of activation and repression	54
14. Differential expression of caspase9 in Notch-perturbed embryos	57

LIST OF FIGURES

1. Recovery of xNBT Expression in ICD-injected embryos	18
2. Recovery of xNBT Expression in DBM-injected embryos	18
3. Neural Cell Counts for GFP-injected embryos	37
4. Neural Cell Counts for ICD-injected embryos	38
5. Neural Cell Counts for DBM-injected embryos	39
6. PCNA Expression in <i>ICD</i> injected embryos	42
7. PCNA Expression in <i>DBM</i> injected embryos	42
8. PCNA Cell Counts for GFP-injected embryos	43
9. PCNA Cell Counts for ICD-injected embryos	44
10. PCNA Cell Counts for DBM-injected embryos	45
11. TUNEL labeling in DBM-injected embryos	47
12. TUNEL labeling in ICD-injected embryos	47
13. TUNEL Cell Counts for GFP-injected embryos	48
14. TUNEL Cell Counts for ICD-injected embryos	49
15. TUNEL Cell Counts for DBM-injected embryos	50
16. Expression of Perp in control embryos	54
17. Expression of Caspase9 in control embryos	54
18. Expression of Caspase7 in control embryos	55
19. Expression of aifm2 in control embryos	55
20. Expression of Caspase9 in Notch-perturbed embryos	58

Chapter 1: Overview of the Problem

The development of functional organ systems during embryogenesis is indisputably a delicate process susceptible to a wide array of disruptions. Environmental and genetic perturbations can profoundly influence developmental pathways and alter the expression of lifelong traits. With many pathways being vulnerable to exogenous and endogenous disruptions, it is not surprising that organisms have evolved the capacity for plasticity in development. The ability to generate functional organs under a wide range of environmental and genetic conditions confers a fitness advantage to the growing organism (Gluckman et al., 2011).

One of the most widely studied systems known to be vulnerable to perturbation in vertebrate development is the central nervous system (CNS). A functional CNS is critical not only for the survival of a mature organism, but also for ensuring the appropriate development of other organ systems. In early embryogenesis, neural development entails the establishment of axis specification, regional identity, cell type identity and synapse formation, all of which involve an intricate array of signaling and transcriptional networks (reviewed by Martynoga et al., 2012). With successful development relying on the careful orchestration of events carried out by complex molecular machinery, the genetic factors involved in the formation of neurons and the primitive CNS must include programs allowing for adaptive responses to environmental disruption and inappropriate signaling. While there has been considerable progress in identifying the genetic pathways governing normal vertebrate neural development, the mechanisms of embryonic response to various perturbations are poorly understood.

The creation and maintenance of balanced neuron and neural progenitor cell populations is a tightly regulated process in development. An adequate supply of neural progenitors is crucial for use in future waves of neurogenesis and brain remodeling and studies of brain development have shown that when this balance is disrupted, severe brain malformations result (Bingham et al., 2003). For example, the generation of a nervous system with an overabundance of neurons has been linked to severe pathologies such as autism (Fang et al., 2014; Courchesne et al., 2007).

Many studies have induced these disturbances through manipulation of Notch juxtacrine signaling, a system responsible for controlling neural progenitor proliferation and the eventual differentiation of neurons. Perturbation of the Notch pathway has been a key method for studying the molecular mechanisms of neurogenesis, due to the role of Notch signaling as a fate switch between progenitor proliferation and neuronal differentiation, as well as ease of pathway manipulation. Previous studies in the Saha lab have shown that, following Notch signaling perturbation, *Xenopus laevis* embryos seem to recover from the well-characterized neurogenic and neural-deficient phenotypes (McDonough, unpublished thesis). The focus of the current study is to elucidate the cellular mechanisms by which the developing *Xenopus* embryo recovers from the imbalance of neural progenitors to mature neurons.

One possible mechanism of restoring population balance is through controlled cell birth and death. Considering their powerful roles throughout development,

apoptosis and cell cycle regulation are likely to serve as the driving forces behind the compensatory response.

Chapter 2: Review of the Literature

2.1 Neural Ectoderm Induction

The earliest stages of *Xenopus* nervous system development begin with the formation of the dorsoventral axis. After egg fertilization, cortical rotation translocates maternal Disheveled protein to the site of the future organizer where it acts to locally stabilize ubiquitous β -catenin. Accumulated β -catenin translocates into the nucleus where it can complex with TCF3 in order to activate expression of dorsalizing genes such as *siamois*. The Siamois protein with Lim-1 subsequently activates expression of the *goosecoid* transcription factor, leading to the formation of the organizer in the future dorsal region of the embryo (Aruga & Mikoshiba, 2011).

Induction of the neuroectoderm then begins during gastrulation. All the cells of the blastula-stage embryo undergo a massive concerted rearrangement, starting from the dorsal lip of the blastopore within the region of the organizer. The cells of the organizer produce neural inducers including Chordin and Noggin, which diffuse into the ectoderm as the organizer tissue involutes and forms the underlying notochord. These neural inducers inhibit the pro-epidermal bone morphogenetic proteins (BMPs) in the dorsal ectoderm and allow specification towards a neural fate (del Corral & Storey, 2001). It has also been proposed that some amount of fibroblast growth factor 4 (FGF4) is required for neural induction along with BMP inhibition. There is additionally a growing body of evidence pointing to calcium as a facilitator of neural induction. Local fluxes in calcium concentration have been observed in gastrulating *Xenopus* embryos (Leclerc et al., 2000) and it has been shown that Noggin elicits a 15% increase in

intracellular calcium concentration within unspecified ectoderm (Moreau et al., 2008; Moreau et al., 1994; Batut et al., 2005). Furthermore, induced intracellular influxes of calcium through calcium channel agonists lead to induction of neural ectoderm (Moreau et al., 1994).

The proneural transcription factors Zic1, Zic3 and SoxD are upregulated in the absence of BMP signals and Zic1 and Zic3 factors are proposed downstream effectors of calcium and FGF4 signaling as well (Leclerc et al., 2003; Marchal et al., 2009). These initial transcription factors activate basic helix-loop-helix (bHLH) transcription factors including neurogenin, which are intermediates in a transcription factor activation cascade leading to the ultimate expression of terminal neural differentiation genes.

2.2 Primary Neurogenesis

Anamniote vertebrate embryos undergo neural development in two stages. The primary nervous system in *X. laevis* serves as a system for basic sensation and movement during the larval stage (Roberts, 2000). Although most primary neurons are replaced during secondary neurogenesis just prior to metamorphosis, primary neurogenesis serves as an excellent model system to study the molecular aspects of neurogenesis due to the simple layout and accessibility of the open neural plate (Wulliman et al., 2005). Many of the genetic players involved in primary neurogenesis are expressed during secondary neurogenesis as well, and are posited to perform similar roles in the secondary system.

Primary neurogenesis begins in *Xenopus* embryos just after gastrulation. Neural stem cells arrange in a bilayered epithelium to form the neural plate (Chalmers et al., 2002). As neural stem cells proliferate, the neural plate expands in preparation for folding into the neural tube. Progenitor cells specified for a neuronal fate are instructively patterned by the spatial distribution of different transcription factors to become specified for a particular neuronal subtype (Guillemot, 2007). Self-renewing specified neural progenitor cells within the neuroectoderm give rise to differentiated neurons. These neurons arise in discrete stripes of *X-ngnr-1* (*Xenopus* homolog of neurogenin) expression promoted by Gli1 at the midline as well as Gli2/3 throughout the neural plate and repressed by stripes of Zic2 expression (del Corral & Storey, 2001). Within these specified zones of neuronal differentiation, neurons appear in a “salt and pepper” pattern exhibiting limited density. This finely tuned spatial pattern of differentiation is achieved through Notch juxtacrine signaling.

2.3 Notch Signaling

The Notch pathway is an ancient and highly conserved mechanism of communication between contacting cells (reviewed by Andersson et al., 2011). Notch signaling between neighboring cells is heavily used throughout development and within many different tissue types. Tissue specificity is likely conferred through the existence of several paralogs, of which there are three in *X. laevis*. The first of these three to be used in development is Notch1, whose expression is restricted to the neural tissue through neurula stages. During *Xenopus* primary neurogenesis, Notch1 signaling provides lateral

fate inhibition by suppressing differentiation in cells contacting differentiating neurons. This functions to prevent both neuronal overcrowding and the depletion of the progenitor pool. The neural determining transcription factor Neurogenin induces the expression of the transmembrane Notch ligand Delta in neural precursors just prior to that of neural differentiation genes. Delta is expressed at low levels across precursor cells, and it is proposed that minute differences in expression among neighbor cells are amplified through a feedback loop wherein pathway activation represses Delta expression and increases Notch expression (Johnston & Desplan, 2010). Delta binds to the extracellular binding site of the transmembrane Notch receptor on a neighbor cell through matching EGF-like repeats. Ligand binding triggers a γ -secretase mediated cleavage of the Notch intracellular domain (ICD) (Schroeter et al., 1998). The ICD translocates to the nucleus where it complexes with Suppressor of Hairless (Su(H)) and Mastermind to activate target genes including *Hes* genes (Iso et al., 2003; Bray & Furriols, 2001). While the mechanism of transcriptional regulation by this complex is still being investigated, the reigning hypothesis proposes that ICD binding inhibits Su(H) activity as a transcriptional repressor (Lubman et al., 2004). The transcription factors encoded by *Hes* target genes act as transcriptional repressors themselves and inhibit the expression of differentiation markers (Artavanis-Tsakonas et al. 1995; Davis et al., 2001; Castro et al. 2005). The signal-receiving cell is thus maintained in the progenitor state. Notch signaling is also a mechanism to instruct neural over epithelial cell fates in *Drosophila* (Kunisch et al., 1994) and has been shown to play a role in glial differentiation later in development as well (Taylor et al., 2007).

The conserved role of Notch signaling as a fate switch in neurogenesis is underscored by studies showing the generation of severe phenotypes from pathway perturbation in *Xenopus*, *Drosophila* and mice. Early experiments seeking to elucidate Notch pathway mechanics in *Drosophila* reported “antineurogenic” phenotypes of neuronal underdevelopment in transgenic flies overexpressing the Notch intracellular domain. Notch-null mutants conversely displayed a neurogenic phenotype in which neuronal markers were expressed beyond the normal bounds of the CNS (Lieber et al., 1993). Chitnis et al. (1995) then investigated the effects of Notch perturbation in *Xenopus* neural development using microinjected RNA transcripts encoding the constitutively active Notch ICD to upregulate Notch signaling. Following perturbation at the two-cell stage, neural plate and early neurula stage embryos (stage 12-17, Nieuwkoop & Faber, 1994) assayed for expression of the pan-neuronal marker *neural tubulin* exhibited a gross depletion of differentiated neurons, indicating that Notch1 hyperactivation inhibits neurogenesis in *Xenopus* embryos as in *Drosophila*. The same study also generated a neurogenic phenotype, detected with whole-mount staining for *n-tubulin*, through injection of RNA encoding a form of *xDelta1* with a truncated intracellular domain posited to downregulate Notch1 signaling (Chitnis et al., 1995).

Several studies have also targeted Su(H) and its homologs to successfully suppress Notch signaling in *Drosophila* and cultured mammalian cells (Li & Baker, 2001; Nakagawa et al., 2000). In the first demonstrated neurogenic phenotype resulting from Notch inactivation in mice, loss of function mutations of the mammalian Su(H) homolog RBP-Jk and Notch1 both led to increased neurogenesis evidenced by expanded

expression of neuronal differentiation markers into neural tissue outside their normal domains at embryonic day 9 (E9) (de la Pompa et al., 1997). Wettstein et al. (1997) similarly downregulated Notch signaling in *X. laevis* using a DNA binding mutant version of xSu(H) that sequesters Notch ICD without affecting transcriptional targets. Following unilateral construct injection at the two-cell stage, the investigators observed a neurogenic phenotype at neural plate stages in which cells expressing *N-tubulin* were overly abundant.

Brain malformation phenotypes in later stages of *Xenopus* were confirmed in the work of Pai et al. (2015), who induced deformities by injecting an unspecified dose of *xNotch1* ICD RNA into the two dorsal blastomeres at the four-cell stage. This resulted in malformed midbrain and nearly absent forebrain observed in whole embryos at stage 45. This study found that endogenous transmembrane voltage patterns are involved in the formation and patterning of neural tissue, and that ICD misexpression leads to depolarization of the characteristically hyperpolarized neural plate. It remains unknown, however, whether this is a direct effect of Notch misregulation or a consequence of overabundant depolarizing progenitor cells.

Although several of these studies on Notch-induced phenotypes describe neural hypertrophy as expanded expression of neuronal markers, few have quantified the effects on cell number within the neural tissue. A study by Coffman et al. (1993) noted that overactivation of Notch signaling in *Xenopus* results in the expansion of neuroepithelial tissue domains, detected with the expression of a neuroepithelial marker, N-CAM, though cells were not counted. Few instances of hypertrophy of CNS

tissue have been observed in *Drosophila* and mice with suppression of Notch signaling. Loss-of-function *Drosophila* mutants displayed tumor-like overgrowth of cells expressing serotonergic markers within the CNS; however, the *sanpodo* (*spdo*) mutant used has been shown to mimic Notch loss-of-function while the *spdo* protein is not involved in Notch-mediated lateral inhibition (Lundell et al., 2003). Neural tissue hypertrophy was also reported upon conditional knockout of the mammalian homolog of Su(H), RBP-Jk, in the hypothalamus of mice. In this study, the region of presumptive arcuate nucleus was visually determined to be enlarged in eosin and hematoxylin-stained histological sections (Aujla et al., 2013).

Finally, Notch signaling has been implicated as a regulator of programmed cell death in brain development, though inconsistent support for its role as an activator or suppressor of apoptosis within the literature indicates a highly context-dependent function. Yang et al. (2004) used cell type specific conditional transgenic constructs to show that Notch1 ICD expression in neural progenitors of transgenic mice led to p53-dependent apoptosis of progenitors, while Notch1 knockout reduced progenitor apoptosis at E9.5 and E10. Another study by Mason et al. (2005) eliminating Notch signaling through conditional knockout showed resultant apoptosis of both neurons and neural progenitors in the brains of mice at E12.5 and E14.5.

2.4 Apoptosis in Neural Development

Programmed death is a universally common fate of cells in development, and is a crucial tool in the elimination of unnecessary, malformed, or transiently functional cells.

In development, apoptosis most commonly occurs within the nervous system, where it is integral to the successful completion of many developmental programs. Apoptosis also appears to be the predominant mode of cell death in neural development over necrosis and autophagy (Arya & White, 2015).

The molecular pathways for enacting programmed cell death are highly conserved in different tissue and developmental contexts; however, the many methods of apoptosis regulation remain an area of active study. Generally, apoptosis may be broken down into intrinsic and extrinsic categories, depending on the source of the triggering signal. Both groupings overlap in their use of certain apoptotic machinery, including caspases and mitochondrial outer membrane permeabilization, but differ in the upstream activation of common cascades.

The functions of apoptosis in neural development vary widely as well. A well-known function of apoptosis is synaptic pruning, which pares down an overabundance of neurons to only those connecting their proper targets (Hamburger et al., 1975). One of the proposed reasons for this strategy is that the structural and synaptic complexity of the vertebrate brain cannot be achieved through genetic programs alone and must employ the use of plastic processes to form a sophisticated and precise network from an initial roughly formed system (Morgensen, 2011). It is hypothesized that the finer mechanisms of this pruning involve the dependence of neurons on target-derived growth factors, neurotrophins, and on synaptic activity to prevent an apoptotic “default” fate (reviewed by Park et al., 2013).

Apoptosis as a means of eliminating transient structures or signaling centers can also have a significant impact in the development of brain morphology. For instance, normal forebrain development has been shown to be dependent on the programmed death of a regionalized subgroup of FGF8-producing cells. The death must occur as part of a spatiotemporal patterning program and when these cells do not die, aberrant FGF8 signaling disrupts gene expression in the developing forebrain and results in structural malformation (Nonomura et al., 2013). The general importance of apoptosis in structuring the brain has been emphasized by other studies showing that mice deficient in apoptosis genes exhibit grossly malformed brain structures (Kuida et al., 1998) and that apoptosis inhibition leads to neural tube closure defects (Yamaguchi et al., 2011).

Should mutations or signaling aberrations affect individual cells or regions of tissue, apoptosis is an essential tool for neutralizing errors in neural development. Ectopic neurons and those with aberrant axon migration or improperly formed connections are destroyed during development. In a more general context, apoptosis has been shown to mitigate the effects of overproliferation in development as well. Hypertrophy of *Drosophila* eye tissue prompted by misexpression of cell cycle regulators E2F and DP triggers an apoptotic response, and excessive proliferation in the syncytial phase of *Drosophila* development is shown to be remedied by apoptosis (Du et al., 1996; Li et al., 1999).

2.5 Cell Cycle Regulation in Neural Development

Differentiated neurons are largely considered to be postmitotic, and while their ability to reenter the cell cycle remains an active area of study, it is generally agreed upon that neurons are nonproliferative, unlike their neural progenitors. New neurons are born, not from the divisions of differentiated neurons, but from the differentiation of neural progenitor cells. This occurs both in neurogenesis during development and in certain regions of the adult brain that harbor adult neural stem cells. Recent findings have shown that neurons do not lack the ability to divide, but instead exercise constant regulation of their cell cycle (Herrup & Yang, 2007). The timing of differentiation and exit of precursors from the cell cycle is highly controlled and has many implications from cell fate to brain size. Cell cycle regulatory genes are therefore common targets of regulation in nervous system development.

Movement through the cell cycle is propelled by the cyclical expression of cyclin and cyclin-dependent kinase (cdk) complexes that enable unidirectional progression through the phases of the cycle and themselves may be regulated by cdk inhibitors. Exit from the cell cycle upon differentiation is mediated through inhibition of the complexes that allow passage through the first gap phase (G1) and commitment to cell division, namely CyclinD/cdk4,6 (Hardwick et al., 2014). Overexpression of complexes allowing progression through G1 such as the G1/S phase cyclinA2/cdk2 complex by unilateral RNA injection in two-cell embryos has been shown to inhibit neuronal differentiation at neural plate stages in *Xenopus*. Interestingly, this study showed that while RNA-injected epidermal tissue displays increased proliferation at tailbud stage, the neural tube in embryos overexpressing cyclinA2/cdk2 shows no difference in proliferation between

control and injected sides, suggesting that endogenous cell cycle cues are capable of overriding exogenous cell cycle influence within neural tissue (Riachard-Parpaillon et al., 2004).

Certain aspects of the cell cycle itself may even play a role in the process of neurogenesis. For example, lengthening of the first gap phase (G1) of the cell cycle is proposed to control the switch from neural progenitor proliferation to differentiation by allowing the accumulation and activity of neurogenic proteins (Hardwick et al., 2014). Inhibition of G1 lengthening through overexpression of the cdk4/cyclinD1 complex in the cortex at E13.5 inhibits neurogenesis while expanding the progenitor population after 24 hours in mice. Lengthening G1 through cdk4/cyclinD1 knockdown conversely stimulates neuronal differentiation (Lange et al., 2009). Research on the link between G1 lengthening and neurogenesis has established that many G1 regulators also impact neurogenesis (Hindley & Philpott, 2012). Cell cycle inhibitors have been shown to regulate differentiation independent of their roles in the cell cycle as well. For instance, overexpression of the cdk inhibitor p27Xic1 in *Xenopus* stimulates neuronal differentiation, while loss of the protein inhibits differentiation. It is thought that p27Xic1 promotes neurogenesis through stabilization of neurogenin (Vernon et al., 2003). Cell cycle manipulation in the context of sequential specification can also affect the composition of neural tissue later in development. In the cortex, where distinct neuronal layers share a “birth date”, early exit from the cell cycle results in reduced populations of later-born neuronal subtypes (Hatakeyama et al., 2004).

Another consequence of cell cycle regulation in neural development is the control of tissue and brain structure size. Precise regulation of the number and timing of progenitor divisions has a large influence on regional or even global tissue expansion. One study showed that increased neural precursor proliferation in the CNS of β -catenin transgenic mice resulted in enlarged brains at E15.5 to such an extent that extra folding of the cerebral cortex was observed (Chenn & Walsh, 2002). The spatial regulation of cell division can also influence the generation of neuronal subtypes. Studies targeting cell cycle regulator cyclin D2 expressed in the cerebellum displayed a lack of differentiated granule cells and stellate interneurons upon gene knockout (Huard et al., 1999).

Neural progenitor cells may even be limited in their capacity to respond to fate-inducing signals depending on their position in the cell cycle. For example, it has been demonstrated that human embryonic stem cells in culture differ in their susceptibility to differentiation cues depending on their cell cycle phase (Pauklin & Vallier, 2013). Peco et al. (2012) suggest that a shortened G2 phase in differentiation-committed cells in chick embryos may limit the Notch-responsive time frame to evade differentiation inhibition.

2.6 Preliminary Studies of Embryonic Response to Notch Perturbation

Prior to this study, preliminary experiments were conducted to determine if the Notch signaling pathway was involved in the establishment of neurotransmitter fate specification (McDonough & Rabe, unpublished). RNA constructs encoding either xNotch1 ICD or xSu(H) DBM were unilaterally injected into a two-cell *X. laevis* embryo,

with the other cell left unperturbed as an internal control. The perturbed embryos were assayed for expression of the panneural marker neural beta-tubulin (NBT) in the control and injected sides using whole mount *in situ* hybridization. In agreement with the literature previously described (Chitnis et al., 1995; Wettstein et al., 1997), these preliminary studies showed that embryos injected with the ICD construct exhibited diminished *NBT* expression on the injected side at neural plate stage. Likewise, DBM-injected sides showed more prominent *NBT* expression at neural plate stages. Gene expression was also examined at the swimming tadpole stage of development. While there was little effect on gene expression for neurotransmitter phenotype markers at these later stages, surprisingly, the difference in *NBT* expression between the injected and non-injected side of the embryo appeared to at least partially resolve (Figs. 1 and 2). A compensatory response resulted in the injected and non-injected sides of the embryo becoming increasingly similar in *NBT* expression for both experimental groups, as detected by whole mount *in situ* hybridization. To assess the levels of persisting transcripts in the embryos with time, Taqman quantitative real time polymerase chain reaction (qRT-PCR) was used. Analysis of qRT-PCR results showed that ICD and DBM RNA construct levels in tailbud stage embryos were still present at 10% of the levels at neural plate stage and persisted at low but still detectable levels into swimming tadpole stages. Thus the apparent compensatory response occurred even with the expression constructs still present within the embryo, albeit at far lower levels per cell. This observation of a compensatory response led to the overarching question of our study: why do certain perturbations result in an amplification of the initial perturbation over

developmental time while others trigger a compensatory response? The specific goal of this study was to determine the molecular mechanisms governing the compensatory response to perturbations in Notch signaling, specifically the role of cell proliferation and programmed cell death.

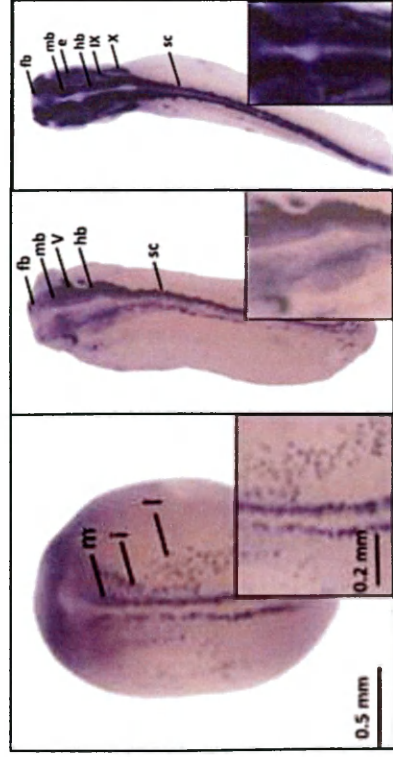


Figure 1. Recovery of xNBT Expression in *ICD*-injected embryos

Embryos injected with *xNotch1 ICD* RNA on the left side at the two-cell stage. Embryos fixed at neural plate (left) tailbud (middle) and swimming tadpole (right) stages and assayed for xNBT expression using *in situ* hybridization. Dorsal view oriented anterior to the top. Abbreviations: m, medial stripe; i, intermediate stripe; l, lateral stripe; fb, forebrain; mb, midbrain; hb, hindbrain; IX, X, cranial nerves; sc, spinal cord. Image courtesy of M. Mcdonough.

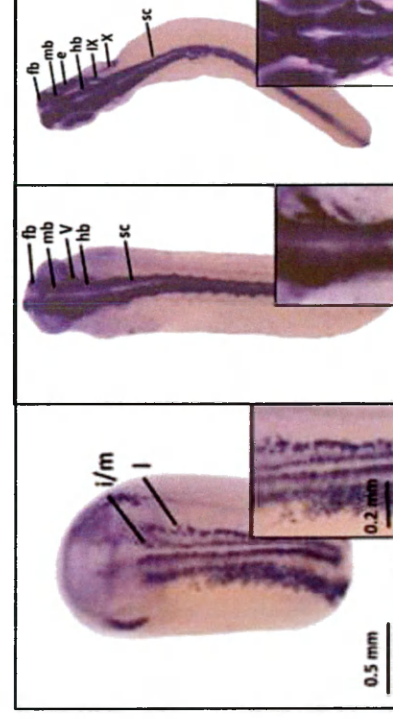


Figure 2. Recovery of xNBT Expression in *DBM*-injected embryos

Embryos injected with *xSu(H) DBM* RNA on the left side at the two-cell stage. Embryos fixed at neural plate (left) tailbud (middle) and swimming tadpole (right) stages and assayed for xNBT expression using *in situ* hybridization. Dorsal view oriented anterior to the top. Abbreviations: m, medial stripe; i, intermediate stripe; l, lateral stripe; fb, forebrain; mb, midbrain; hb, hindbrain; IX, X, cranial nerves; sc, spinal cord. Image courtesy of M. Mcdonough.

Chapter 3: Experimental Overview and Hypotheses

As this literature review indicates, proper formation of a functional nervous system relies heavily on the execution of genetically programmed sequences but also on the embryo's ability to be responsive during development, should something go awry. As previously discussed, both apoptosis and cell cycle regulation are major contributors in central nervous system development. We therefore hypothesized that they are mechanisms of compensatory remodeling in response to early Notch perturbation. This project aimed to investigate the roles of apoptosis and cell cycle regulation in the normalization of cell type distribution during early CNS development. This was first achieved by examining whether the responsive process involved changes in cell number. We predicted that, in response to hyperactive or suppressed Notch, disparities in neural cell number would equalize over time between injected and control tissues of the same embryo. To investigate whether recovery from Notch perturbation in the early CNS involved changes in cell number, embryos were first unilaterally injected with RNA constructs encoding either the Notch intracellular domain (ICD) or a DNA-binding mutant of Suppressor of Hairless (DBM) at the two-cell stage. Transverse sections of perturbed embryos' neural tissue were stained with DAPI to label the DNA within nuclei of individual cells, and cell totals were counted and compared between injected and control halves of each embryo.

To investigate the role of apoptosis and cell cycle regulation, construct-injected embryos were assayed for expression of the proliferation marker proliferating cell nuclear antigen (PCNA) and for the presence of apoptosis-induced nicked DNA through

terminal deoxynucleotidyl transferase dUTP nick-end labeling (TUNEL). Cells positive for PCNA and TUNEL were counted from transverse sections and totals were compared between injected and control conditions. Assays and cell counts were performed on embryos at stages within the time course of the preliminary study, with two intermediate late stages added to observe the timing of compensation on a finer scale. We predicted that where there were differences in neural cell number there would be a compensatory pruning or expansion of cell populations in the injected tissue (Table 1).

In order to examine the role of specific apoptotic pathways in the compensation process, various genes involved in both intrinsic and extrinsic pathways were selected for study. Candidate genes (Table 2) were cloned and antisense RNA probes were synthesized for each. The developmental and functional expression of each was profiled with whole mount *in situ* hybridization of control and construct-injected embryos. Localized expression and differential regulation were assessed through histological analysis of the nervous tissue. It was hypothesized that apoptotic factors employed in the compensation program would exhibit differential expression between control and perturbed halves of brain and spinal cord tissue. All studies of construct-injected embryos also included vehicle-injected controls to control for the effects of microinjection.

Construct	Predicted Phenotype	Predicted Response
Notch ICD	Decreased neuron population	Increased neuronal differentiation
	Increased progenitor population	Increased progenitor apoptosis Decreased progenitor division
Su(H) DBM	Increased neuron population	Increased neuron apoptosis Decreased neuronal differentiation
	Decreased progenitor population	Increased progenitor division

Table 1. Predicted Notch perturbation phenotypes and compensatory responses.

Chapter 4: Materials and Methods

Animal Care

All animal care and embryo collection procedures are in accordance with and approved by the William & Mary Institutional Animal Care and Use Committee (IACUC). Adult *Xenopus laevis* were housed in Nalgene plastic tanks containing well water with uniodized NaCl added to a final concentration of 20mM and kept in temperature-controlled rooms with a programmed 14:10 light-dark cycle. Males and females were housed separately at a maximum density of 12 and 8 frogs per tank, respectively, and were fed ad libitum Nasco Adult Frog Pellets three times per week. Tanks were cleaned by flushing with fresh well water for a minimum of three hours, one hour after adults were fed.

Embryo Production and Collection

Embryos were obtained through natural matings with isolated adult pairs induced with human chorionic gonadotropin (hCG). Approximately 12 hours before anticipated embryo collection, *X. laevis* males and females were injected subcutaneously with 400 and 600 units of hCG, respectively (Sive et al. 2007). Either one or two induced pairs were placed in a mesh-bottom container suspended over removable plastic trays in an isolated glass tank for convenient embryo retrieval. Embryos were collected in trays and embryo jelly coats were removed using the following procedure. Tank water was decanted off the embryo tray and replaced with 100 ml solution of 2% L-cysteine in 0.1X Marc's Modified Ringer's (MMR) brought to pH

8 with NaOH. After a maximum of 5 minutes in cysteine solution with gentle agitation, embryos were rinsed three times in 0.1X MMR containing gentamicin and aliquotted into 100mm glass petri dishes containing 0.1X MMR + 50 mg/ml gentamicin at a maximum density of 100 embryos per plate. Embryo plates were sorted to remove unfertilized or necrotic embryos 1.5 hours after collection and stored in incubators ranging from 14°C to 23°C with daily solution changes. Embryos needing to be discarded prior to neurula stages were isolated and treated with 70% ethanol for 5-10 minutes before disposal. After neurula stage, embryos to be discarded were anesthetized with 0.5 mg/ml tricaine methanesulfonate (MS222, Sigma-Aldrich) prior to ethanol treatment.

Notch Perturbation Constructs

Constructs were kind gifts of C. Kintner (Wettstein et al., 1997). Plasmid DNA was transformed into DH5 α hosts and, following growth in liquid culture, DNA was recovered using either the Promega PureYield Plasmid Midiprep kit or the Macherey-Nagel NucleoBond Xtra Midi kit following the manufacturers' instructions. DNA purity and concentration was assessed using a Nanodrop spectrophotometer. A diagnostic restriction digest was performed using restriction endonucleases targeting sites flanking the clone insert. Samples of digested products and uncut plasmid DNA were electrophoresed on a 1.5% agarose gel to confirm clone identity and DNA quality. Midiprep DNA was stored at 4°C.

Synthesis of Capped RNA for Microinjections

Capped sense RNA was synthesized from the sources listed in Table 2 using the mMessage mMachine kit (Ambion). Following the manufacturer's instructions, reaction mixtures consisted of 1 µg linearized template DNA, 10 µl 2X NTP/CAP mix, 2 µl 10X Reaction Buffer, 2 µl of enzyme mix containing appropriate RNA polymerase (Table 2), and nuclease free water (NFW) to a total volume of 20 µl. Reactions were incubated at 37°C for 2 hours followed by a 15 minute incubation with 1 U TURBO DNase at 37°C. Synthesized RNA was purified using the RNeasy MinElute Cleanup kit (Qiagen) according to the manufacturer's protocol.

Sample volume was brought to 100 µl with nuclease-free water and 350 µl of Buffer RLT was added. Following addition of 250 µl of 100% EtOH, the mixture was placed in an RNeasy spin column and centrifuged for 15 seconds at 16,100 x g. The column was placed in a fresh 2 ml collection tube and 500 µl of Buffer RPE was added to the column. After an identical centrifugation step, flowthrough was discarded and 500 µl of 80% EtOH was added to the column before centrifuging for 2 min at 16,100 x g. The spin column was then transferred to a fresh 2 ml collection tube and centrifuged for 5 minutes with the cap open to rid the column membrane of additional ethanol. Once transferred to a 1.5 ml collection tube, the sample was eluted with 14 µl RNase-free water, allowed to sit for one minute, and centrifuged for 1 minute at 16,100 x g. The eluate was passed through the membrane once more in an identical manner and the final sample was placed on ice during quality assessment. RNA yield was assessed using a Nanodrop spectrophotometer and quality was checked with gel electrophoresis on a

1.5% agarose gel as previously described. Capped RNA was divided into single-use 1 μ l aliquots and stored at -20°C.

Microinjections

Glass needles for microinjections were made from 7 inch glass capillary tubes (Drummond) pulled twice in a Narishige PB-7 needle puller. Needle tips were poked gently through a taut sheet of single-ply bath tissue to produce a beveled tip 10-30 μ m in diameter. Dejellied embryos were placed in a 30 mm clay-lined plastic petri dish with indented rows for spacing embryos. Injection dishes were filled with 0.33X MMR with 4% ficoll (GE Healthcare) [for added viscosity]. Glass needles filled with mineral oil were mounted on a Nanoject II microinjector (Drummond) and loaded with injectable RNA synthesized *in vitro* as previously described. Embryos were unilaterally injected at the two-cell stage into the animal cap with 4.6 nl of nuclease-free water (NFW) containing 1.5 ng of RNA encoding either Notch intracellular domain (ICD) or a DNA-binding mutant of Suppressor of Hairless (DBM) along with 0.5 ng of RNA encoding either green fluorescent protein (GFP) or beta galactosidase (β -gal) for use as injection tracers. Vehicle-injected control embryos were administered 4.6 nl injections of NFW containing 0.5 ng of *GFP* or β -gal RNA in NFW.

Following injection, embryos were transferred to a plastic 100 mm petri dish and allowed to recover for a minimum of 2 hours in 0.33X MMR + 4% ficoll. Injected embryos were then transferred to fresh dishes containing 0.1X MMR + 4% ficoll and

kept in incubators ranging 14°C to 23°C. Following gastrulation, injected embryos were kept in 0.1X MMR + 50 mg/ml gentamicin.

Embryo Fixation

Embryos were raised to the desired stages identified using the Nieuwkoop and Faber (NF) staging guide (1994) and fixed using one of the following procedures specific for either GFP or β -gal traced embryos. Embryos injected with GFP RNA were viewed under a fluorescent stereoscope and fluorescing embryos were sorted into left- or right-injected groups. Embryos were removed from their vitelline sheath using fine forceps and prior to NF stage 20 the archenteron was pierced with a glass needle. GFP-traced embryos were then fixed for 90 minutes in 1X MEMFA solution (MOPS/EGTA/Magnesium sulfate/Formaldehyde buffer) at room temperature, rinsed twice in 100% EtOH and stored in fresh 100% EtOH at -20°C. Embryos injected with β -gal were fixed for 30 minutes at room temperature in 1X MEMFA, rinsed for 5 minutes in 1X PTw, and incubated in 500 μ l of color developing solution containing 25 μ l 0.1M ferricyanide, 25 μ l 0.1M ferrocyanide, 10 μ l 0.1M magnesium chloride, and 5 μ l of 100 μ g/ml Red-Gal in 1X PTw until red staining developed. Stained embryos were fixed for an additional 90 minutes in 1X MEMFA at room temperature, washed twice with 100% EtOH and stored at -20°C in fresh 100% EtOH. All embryos to be fixed after neurulation were anesthetized with MS222 prior to fixing.

TUNEL Apoptosis Assay

In order to identify cells undergoing apoptosis, whole mount TUNEL assays were conducted on RNA-injected embryos fixed at various developmental stages. Embryos were first rehydrated in successive 5 minute washes of 75% EtOH in sterile double distilled water (sdd water), 50% EtOH in sterile distilled water, 25% EtOH in PBT, and 100% PBT followed by three 20 minute washes in 100% PBT. Embryos were then incubated for 2 hours in 100 μ l TdT buffer composed of 80 μ l PBS and 20 μ l 5X TdT buffer (Invitrogen). TdT buffer was replaced with TdT reaction mix composed of 100 μ l 1X TdT Buffer, 0.2 μ l Dig-dUTP, and 2 μ l TdT enzyme (Invitrogen). Following a 12 hour incubation at room temperature, the reaction was stopped with two 1 hour incubations in 1mM EDTA in PBS at 65°C. Embryos were then washed 5 times for 10 minutes each in 1X PBT and blocked for 1 hour in 500 ml of 2% BMB blocking reagent (Roche) in maleic acid buffer (MAB). The embryos were incubated at 4°C overnight in a solution of 0.25 μ l anti-digoxigenin alkaline phosphatase-coupled antibody (Roche) in 500 μ l of 2% BMB in MAB. After incubation, embryos underwent five 1 hour washes in MAB followed by two 5 minute washes in alkaline phosphatase (AP) buffer made of 2.5 ml 1M Tris buffer, 1.25 ml 1M magnesium chloride, 0.5 ml sodium chloride, 25 μ l Tween-20, 0.012 g levamisole, and sdd water to a final volume of 25 ml. Color was developed by incubating embryos for 30 minutes in 1 ml of AP buffer containing 4.5 μ l nitro-blue tetrazolium and 3.5 μ l 5-bromo-4-chloro-3-indolyl phosphate (Promega). Reactions were fixed at 4°C for at least 12 hours in 1X MEMFA, washed for 5 minutes in 1X PBS and stored at 4°C in fresh 1X PBS.

Whole Mount in situ Hybridization

Whole mount *in situ* hybridization was performed to analyze spatial gene expression in whole embryos as described. Fixed embryos were rehydrated by successive 5 minute washes in 100% ethanol, 75% ethanol in sdd water, 50% ethanol in sdd water, 25% ethanol in PTw, and 100% PTw. Following three 5 minute washes in 100% PTw, embryos were permeabilized in 1 ml of 10 µg/ml proteinase K for 30 minutes with nutation. Following two 5 minute rinses in 0.1M triethanolamine, acetic anhydride was added to neutralize positive charges within the tissue and prevent nonspecific RNA probe binding in subsequent steps. Following two 5 minute washes in PTw, permeabilized embryos were refixed with 4% paraformaldehyde in 2X PTw. Excess paraformaldehyde was removed with three 5 minute washes in 100% PTw and embryos were prehybridized in *in situ* hybridization buffer (ISH buffer) for a minimum of 6 hours at 60°C with agitation. ISH buffer was replaced with 1 ng/µl RNA probe, synthesized as previously described, and embryos were left to hybridize at 60°C for 8-15 hours. RNA probes were recovered and stored (for reuse no more than 3 times) and replaced with ISH buffer for a 10 minute incubation at 60°C. Hybridized embryos were washed in 2X SSC at 60°C three times for 20 minutes. Embryos were treated for 30 minutes with 20 µg/ml RNase A in 2X SSC at 37°C to degrade unbound probe, then washed twice in 2X SSC for 10 minutes at room temperature and twice in 0.2X SSC for 30 minutes at 60°C. Embryos were then washed twice in MAB for 15 minutes and incubated in 2% BMB in MAB for 1 hour at room temperature to prevent nonspecific antibody binding in subsequent steps. Following this blocking step, embryos were incubated with a 1:2000

dilution of AP coupled anti-digoxigenin antibody in 2% BMB in MAB for 8-15 hours at 4°C with nutation. Excess antibody was washed away with four 1 hour MAB washes and one overnight MAB wash at 4°C with nutation. Embryos were washed twice for 5 minutes with AP buffer and then incubated in 1 ml of AP buffer containing 4.5 µl nitro-blue tetrazolium and 3.5 µl 5-bromo-4-chloro-3-indolyl phosphate (Promega) until sufficient staining developed. Color reactions were stopped by fixing in 1X MEMFA for 12 hours at 4°C and subsequently washed in 1X PBS for 5 minutes before storing at 4°C in fresh 1X PBS. Each *in situ* hybridization experiment was performed with a positive control using a previously tested probe.

Whole Mount Photography

Brightfield photographs documenting the results of TUNEL or *in situ* hybridization assays on whole embryos were taken with an Olympus DP71 camera mounted on an Olympus SZH10 stereoscope using DP Controller software (Olympus). Group and representative single-embryo images were photographed in a paraffin-lined glass petri dish filled with 1X PBS. Embryos were then cleared for improved signal visualization in benzyl benzoate; benzyl alcohol (2:1) following dehydration by three 10 minute washes in 100% methanol; embryos were then re-photographed.

Cryosectioning

Histological analysis of assayed embryos was performed through cryosectioning on a Cryostar NX70 instrument. Embryos were first fixed in 1.6M sucrose for a minimum

of 12 hours and placed in Tissue Freezing Medium (TFM, Triangle Biomedical Sciences) for at least 1 hour prior to sectioning transverse 18 μ m sections along the anterior-posterior body axis. Individual sections were placed on glass slides that had been dipped three times in a 50 ml solution containing 0.15 g KNOX gelatin and 0.025 g chromium potassium sulfate. Slides were left to dry for at least 12 hours before coverslipping.

Sections that were used for cell counts were stained with the fluorescent DNA dye DAPI and coverslipped with minimal light exposure. To do so, TFM was removed from the sections with a 10 minute wash in 1X PBS followed by staining for 15 minutes in DAPI solution (Sigma Aldrich). Excess DAPI was washed away in another 10 minute 1X PBS wash and slides were rinsed for 5 minutes in dd water. Slides were dried and glass coverslips were affixed with Fluoromount G mounting medium (Southern Biotech).

An alternative protocol was used to remove TFM, dehydrate and fix tissue to slides for sections not requiring DAPI staining. Slides were taken through the following series of washes: 1 minute in 1X PBS, 3 minutes in 4% PFA in PBS, 3 minutes in 1X PBS, 1 minute in deionized water, 1 minute in 95% ethanol, 1 minute in 100% ethanol, and 5 minutes in Citrisolv (Fisher). Dried slides were coverslipped with Permount (Fisher).

Slides were brightfield imaged with either an Olympus QColor 5 or AmScope camera on a BX60 microscope (Olympus) using QCapture Pro or AmScope software. Sections used in cell counting were photographed using a UV burner to produce fluorescent DAPI images.

Cell Counting

Left and right halves of neural tissue were manually outlined as regions of interest (ROIs) on brightfield or fluorescent DAPI images using ImageJ and saved as .roi files (Helmy & Azim, 2012). A second group of ROIs corresponding to regions with *in situ* hybridization signal within neural tissue were generated. Each group of ROIs was overlaid onto their respective DAPI images and cells were identified and counted using an image-based tool for counting nuclei (ITCN). TUNEL-positive cells were counted using brightfield images.

Notch Perturbation Microarray Analysis

Following preliminary studies on the effects of perturbation of the Notch signaling pathway, microarray analysis was used to identify genes involved in the embryonic response (Vasiliu et al., 2015). Perturbed embryos were obtained as previously described and an Affymetrix GeneChip was used to evaluate differential gene expression between ICD- and DBM-injected embryos at NF stage 28. Initial candidate genes were selected from the results of this microarray. Microarray results containing the probe sequence, p value, and fold change in expression were ranked by p value and the two thousand entries with greatest statistical significance were annotated with function using information from Genbank. Nucleotide sequence alignments were generated for each Affymetrix probe using the basic local alignment search tool (BLAST, NLM) and a matching gene name, accession number, and alignment E value were

recorded. Gene name abbreviation, function, and functional category (e.g. apoptosis, cell division cycle) were also recorded.

RNA Extraction

Total RNA was extracted from whole embryos flash frozen at the developmental stage of interest using the following method. Frozen embryos were homogenized in 350 μ l TriReagent (MRC) using a plastic pestle. The homogenate was then combined with 17.5 μ l of phase separation reagent BAN (MRC) and shaken vigorously for 15 seconds. The sample was incubated at room temperature for 5 minutes and centrifuged at 4°C for 15 minutes at 21,000x g. The aqueous phase containing extracted RNA was transferred to a fresh microcentrifuge tube and combined with an equal volume of 70% ethanol. Extracted RNA was then purified using the Qiagen RNeasy mini kit. The sample was transferred to an RNeasy mini spin column and centrifuged at 16,100 x g at room temperature for 15 seconds. Column flowthrough was discarded and 700 μ l of RW1 was added to the column. After centrifugation for 15 seconds at 16,100 x g at room temperature, flowthrough was discarded and 500 μ l RPE was added to the column. Following another such centrifugation, an additional 500 μ l RPE was added. After a final centrifugation, the column was transferred to a fresh 2mL collection tube and centrifuged for 1 minute at 16,100 x g at room temperature. The column was placed in a fresh 1.5ml microcentrifuge tube and RNA was eluted with 30 μ l nuclease-free water. The eluate was passed through the column a second time following a one minute incubation to increase yield.

RNA yield and purity was assessed with the Nanodrop spectrophotometer using ND-1000 software. Extracted RNA quality was assessed with gel electrophoresis on 1% agarose gels containing 3 μ l of 10 mg/ml ethidium bromide intercalating dye. 12 μ l samples containing 1 μ g of nucleic acid in 1X DNA dye were loaded into lanes alongside 10 μ l of the 1 Kb Plus DNA Ladder size standard (Life Technologies). Gels were placed in an electrophoresis chamber, submerged in 1X TAE, and run for 30 minutes at 170V. Bands were transilluminated in a FluorChem HD2 ultraviolet light cabinet (Alpha Innotech) and imaged using FluorChem software. Following quality assessment, extracted RNA was stored at -80°C.

Synthesis of cDNA

cDNA for use in polymerase chain reactions (PCR) was synthesized using the BioRad iScript Advanced cDNA Synthesis kit following the manufacturer's instructions. One microgram of *X. laevis* total RNA from a single developmental stage was combined with 4 μ l of 5X iScript reaction mix and 1 μ l of iScript reverse transcriptase and brought to 20 μ l with nuclease-free water. The reaction was then cycled in a thermocycler according to the kit manufacturer's protocol as follows: 5 minutes at 25°C; 60 minutes at 42°C; 5 minutes at 85°C; hold at 4°C. Synthesized cDNA was stored in single-use 1 μ l aliquots at -80°C.

Cloning of Candidate Genes

In order to clone genes of interest identified from the microarray experiment and other potentially relevant genes, primers for each candidate gene targeted 500-1420 bp regions of the known cDNA. Forward and reverse primers were designed with Primer3 using default settings with an optimal length of 20 bp, T_m of 60°C and GC content of 50%. Whenever possible, primers were designed to span an exon-exon boundary to control for genomic DNA contamination. Annotated sequences for each gene were obtained from Xenbase.org. Primers were ordered as oligonucleotides from IDT and brought up in 1X TE to a stock concentration of 1 mM to be stored at -80°C; primers to be used in PCR were brought to a working dilution of 10 μ M with nuclease-free water.

PCR was performed using cDNA synthesized from the extracted RNA of *X. laevis* embryos at a single developmental stage as previously described. Reactions consisted of 1 μ l forward primer, 1 μ l reverse primer, 1 μ l cDNA and 22 μ l Platinum PCR Supermix (Life Technologies). Reactions were incubated in a thermocycler using the manufacturer's suggested protocol, with an additional 1 minute during elongation at 72°C per Kb of target product. PCR product size and quality were assessed using gel electrophoresis with a 1-1.5% agarose gel. PCR products were stored at 4°C for a maximum of 24 hours before use in vector ligation to avoid degradation.

Successfully amplified fragments were ligated into the pSC-A-amp/kan vector using the StrataClone PCR Cloning Kit. Briefly, 2 μ l of a 1:10 dilution of PCR product was combined with 1 μ l of StrataClone vector mix and 3 μ l StrataClone cloning buffer and

incubated for 5 minutes at room temperature to allow ligation by topoisomerase I.

Ligated vector was either stored at -20°C or used immediately for transformation into *E. coli*.

Ligated vector was then transformed into thawed StrataClone SoloPack competent cells using the manufacturer's protocol. Following at least a one hour recovery period in Luria broth (LB), transformed cells were plated on LB-ampicillin plates spread with 2% X-gal for color-screening. Plates were inverted and incubated at 37°C for at least 12 hours to allow colony growth. White transformed colonies were selected for overnight growth in liquid culture media.

Plasmid Isolation

Miniprep cultures were incubated in 4 ml of LB containing 50 µg/µl ampicillin for at least 12 hours at 37°C with agitation and 50% glycerol stocks were made by combining 500 µl sterile glycerol with 500 µl culture and stored at -20°C. Plasmids were recovered using the Promega Wizard Plus Miniprep kit following the manufacturer's instructions. Isolated plasmid was subjected to preliminary restriction endonuclease digests to confirm insert identity by cleaving the plasmid at two specific restriction sites flanking the clone insert (see Table 1). Restriction digest products were run on a 1% agarose gel to validate the presence of predicted fragment size. Clone identity was confirmed via Big Dye sequencing using M13 forward and reverse sequencing primers.

Liquid cultures were then grown as previously mentioned from selected miniprep glycerol stocks for midiprep plasmid isolation. Turbid cultures were used to

make 15% and 50% glycerol stocks which were stored at -80°C and -20°C, respectively.

Midiprep plasmid DNA was isolated using either the Promega PureYield Plasmid Midiprep kit or the Macherey-Nagel NucleoBond Xtra Midi kit following manufacturers' instructions and assessed for quality and concentration as previously described.

Diagnostic digestion with restriction endonucleases was used to confirm clone identity as described above.

Gene Name	Vector	Flanking Restriction Sites	Restriction Endonuclease for Linearization	RNA Polymerase for Transcription
<i>perp</i>	pSC-A-amp/kan	EcoRI	HindIII	T7
<i>tp53</i>	pSC-A-amp/kan	EcoRI	BamHI	T3
<i>bcl2</i>	pSC-A-amp/kan	SacI	NotI	T3
<i>bax</i>	pSC-A-amp/kan	EcoRI	XbaI	T3
<i>caspase3</i>	pSC-A-amp/kan	NcoI	NotI	T3
<i>caspase6</i>	pSC-A-amp/kan	HpaI, ClaI	ClaI	T7
<i>caspase9</i>	pSC-A-amp/kan	NcoI	NotI	T3
<i>caspase7</i>	pSC-A-amp/kan	EcoRI	XbaI	T3
<i>aifm2</i>	pCMV-SPORT6.ccdB	NotI, KpnI	KpnI	T7
<i>endog</i>	pCMV-SPORT6.ccdB	EcoRI, XhoI	EcoRI	T7
<i>nucβ-gal</i>	pCS2+	NotI, BamHI	NotI	SP6
<i>gfp</i>	pCS2+MT	EcoRI, NotI	NotI	SP6
<i>Notch1 ICD</i>	pCS2+MT	EcoRI, XbaI	NotI	SP6
<i>xSu(H) DBM</i>	pCS2+	BamHI, XhoI	NotI	SP6

Table 2. Constructs for capped RNA and RNA probe synthesis.

Chapter 5: Results

5.1 Effects of Notch Perturbation on Cell Number

To probe for a possible role of apoptosis and cell cycle regulation in the compensatory response observed in preliminary *xNBT in situ* hybridization experiments, (McDonough, unpublished), we first investigated the effects of Notch perturbation on neural cell number. We hypothesized that Notch perturbation would result in imbalanced neural cell numbers between perturbed and unperturbed tissue that would equalize through varied levels of apoptosis and proliferation over time. As with the initial NBT experiments, we began by unilaterally injecting *in vitro* synthesized RNA constructs into embryos at the two-cell stage to overexpress key components of the Notch signaling pathway. We upregulated Notch signaling with the administration of sense transcripts for *xNotch1 ICD*, which encodes the intracellular portion of the Notch receptor that undergoes nuclear import to ultimately affect target gene transcription (Chitnis et al., 1995). To attenuate Notch signaling we introduced sense RNA transcripts encoding a DNA binding mutant (DBM) Suppressor of Hairless, a key protein in the transcriptional activation complex formed with Notch ICD (Wettstein et al., 1997). The DBM protein complexes with ICD but does not bind DNA, acting to sequester the signal. Each transcript was co-injected with RNA for green fluorescent protein (GFP) or β -galactosidase (β -gal) to track injection sidedness. This unilateral injection method provided a convenient internal control for comparison at every stage of analysis.

Injected embryos were fixed at neural plate (15), tailbud (25), late tailbud (30), swimming tadpole (35), and late tadpole (40) stages and transversely sectioned along

the anterior-posterior axis. Sections stained with DAPI were imaged and used to count the total number of cells within the neural tissue of experimental and control sides of each embryo. Cell totals for each side were normalized by the number of sections for that embryo to control for differences in embryo size and slight developmental variance.

Vehicle-injected control embryos, administered RNA encoding a tracer protein only, displayed no significant difference in neural cell number at any stage (Table 3). Embryos injected with the *xSu(H) DBM* construct also showed no significant difference in neural cell number at any stage (Fig. 5). Embryos injected with *xNotch ICD*, however, had significantly more neural cells on the injected side compared to the internal control from neural plate stage 15 through swimming tailbud stage 35 stages (Table 4, Fig. 4).

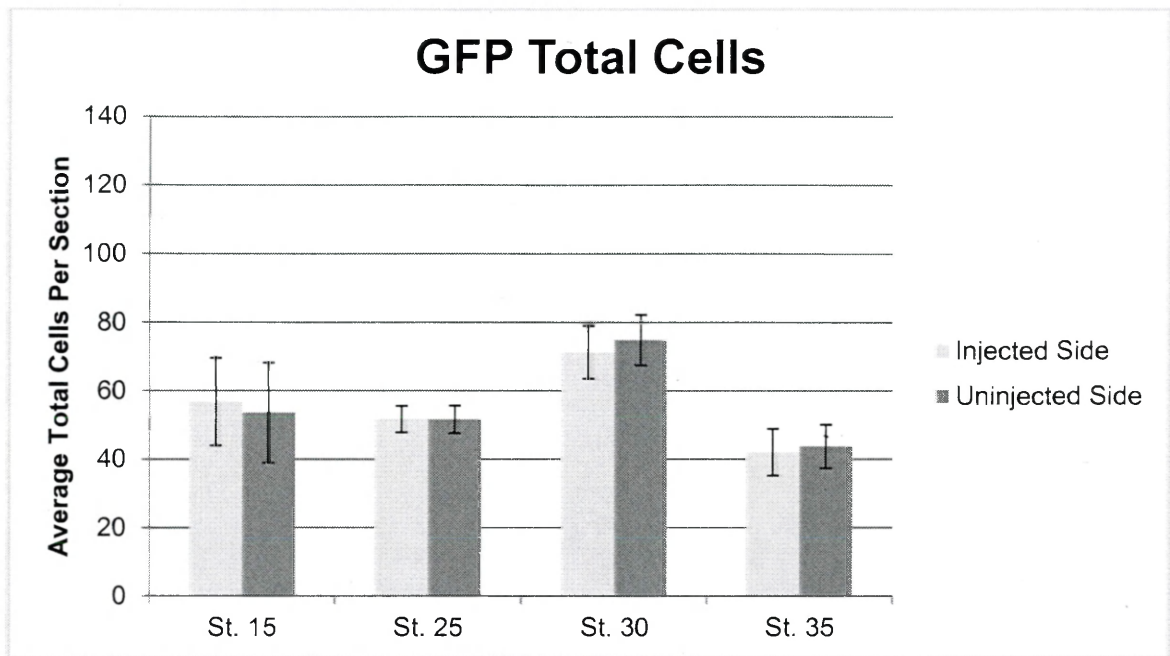


Figure 3. Neural Cell Counts for GFP-injected embryos.

Embryos were unilaterally injected at the two-cell stage with 0.5 ng of either GFP or β -galactosidase RNA as an injection control. Embryos were fixed at the stages on the x-axis and transverse 18 μ m sections were taken along the anterior-posterior axis. Tissue was stained with DAPI and individual cells were counted in the injected and control halves of the neural tissue. Bars represent the average total number of neural cells in each side normalized to the number of sections for the corresponding embryo. Error bars represent one standard deviation.

Table 3. Neural Cell Counts for GFP-injected embryos.

Stage	Total cell average- Injected Side	standard deviation	Total cell average- Uninjected Side	standard deviation	p value (n=10)
St. 15	56.8	25.6	53.6	29.2	0.540
St. 25	51.7	7.75	51.6	8.01	0.987
St. 30	71.2	15.4	74.8	14.8	0.092
St. 35	42.0	13.6	43.7	12.7	0.206

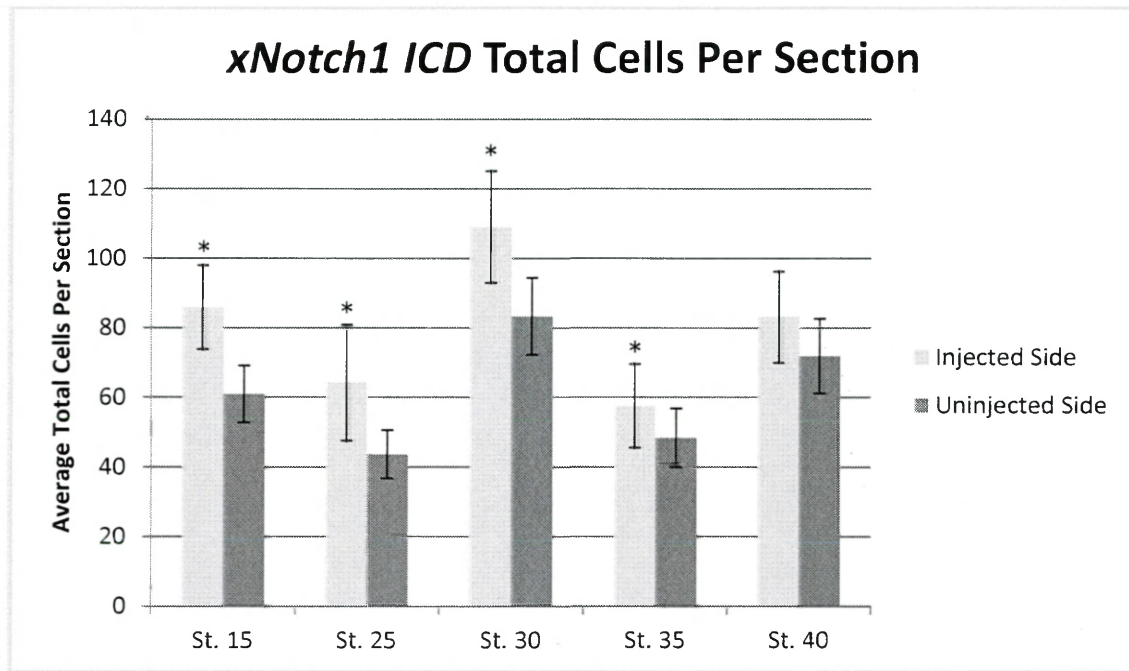


Figure 4. Neural Cell Counts for ICD-injected embryos.

Embryos were unilaterally injected at the two-cell stage with 1.5 ng *xNotch1* ICD RNA and 0.5 ng of either GFP or β -galactosidase RNA as an injection tracer. Embryos were fixed at the stages on the x-axis and transverse 18 μ m sections were taken along the anterior-posterior axis. Tissue was stained with DAPI and individual cells were counted in the injected and control halves of the neural tissue. Bars represent the average total number of neural cells in each side normalized to the number of sections for the corresponding embryo. Error bars represent one standard deviation. Asterisk indicates statistical significance ($p < 0.05$).

Table 4. Neural Cell Counts for ICD-injected embryos.

Stage	Total cell average- Injected Side	standard deviation	Total cell average- Uninjected Side	standard deviation	p value (n=10)
St. 15	85.9	24.1	60.9	16.3	0.000
St. 25	64.2	33.3	43.6	13.8	0.011
St. 30	109.0	32.2	83.3	22.1	0.001
St. 35	57.6	24.1	48.4	16.9	0.021
St. 40	83.1	26.3	71.9	21.5	0.068

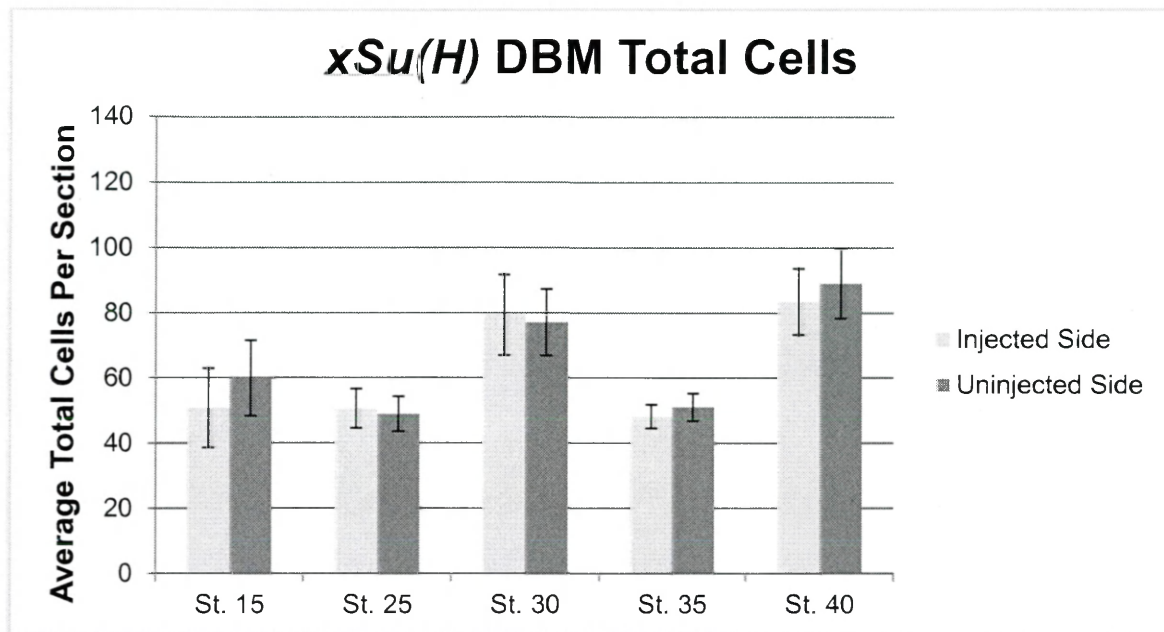


Figure 5. Neural Cell Counts for DBM-injected embryos.

Embryos were unilaterally injected at the two-cell stage with 1.5 ng xSu(H) DBM RNA and 0.5 ng of either GFP or β -galactosidase RNA as an injection tracer.

Embryos were fixed at the stages on the x-axis and transverse 18 μ m sections were taken along the anterior-posterior axis. Tissue was stained with DAPI and individual cells were counted in the injected and control halves of the neural tissue. Bars represent the average total number of neural cells in each side normalized to the number of sections for the corresponding embryo. Error bars represent one standard deviation.

Table 5. Neural Cell Counts for DBM-injected embryos.

Stage	Total cell average- Injected Side	standard deviation	Total cell average- Uninjected Side	standard deviation	p value (n=10)
St. 15	50.8	24.3	59.9	23.1	0.182
St. 25	50.6	12.1	48.9	10.6	0.264
St. 30	79.3	24.8	77.1	20.3	0.476
St. 35	48.2	7.24	50.9	8.36	0.132
St. 40	83.5	20.4	88.9	21.3	0.078

5.2 Effects of Notch Perturbation on Cell Proliferation

In order to assess the involvement of cell cycle regulation in the compensatory response, we first examined whether the proportion of proliferating cells differed between injected and control sides of Notch-perturbed embryos. Embryos were unilaterally injected as before with either *xNotch1 ICD* or *xSu(H) DBM* and an injection tracer at the two-cell stage. Vehicle-injected controls were administered tracer RNA only to control for the effects of injection. Embryos fixed at neural plate, tailbud, late tailbud, swimming tadpole, and late tadpole stages were assayed for expression of proliferating cell nuclear antigen (PCNA), a DNA clamp required in DNA replication, through whole mount *in situ* hybridization (Wulliman et al., 2005). Embryos transversely sectioned along the anterior-posterior axis were stained with DAPI and PCNA-positive cells within the neural tissue on each side were counted. Total positive cells for each side were normalized by the total number of neural cells for that side of the embryo to control for tissue size.

Vehicle-injected control embryos exhibited no significant difference in PCNA expression between experimental and control sides at any stage investigated (Fig. 8). Embryos injected with *xSu(H) DBM* RNA showed significantly more cells expressing PCNA on the uninjected control side at neural plate stage 15 ($p=0.006$, $n=5$), stage 30 late tailbud ($p=0.014$, $n=5$), and stage 35 swimming tadpole ($p=0.038$, $n=5$) (Fig. 10, Table 8). Embryos injected with *xNotch1 ICD* exhibited a higher proportion of cells with PCNA expression on the uninjected control side at late tailbud stage 30 ($p=0.009$, $n=5$)

(Fig. 9, Table 7). Representative histological images of *DBM* and *ICD embryos* at each developmental stage assayed are shown in Figures 6 and 7.

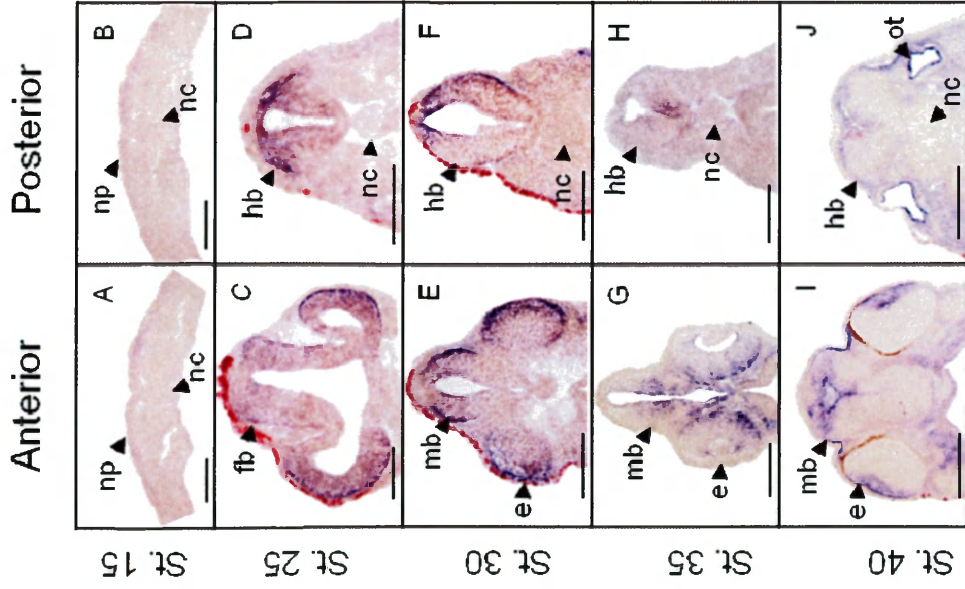


Figure 6. PCNA Expression in ICD injected embryos
 Histological analysis of PCNA expression (purple staining) detected by *in situ* hybridization in embryos unilaterally injected with 1.5 ng xNotch1 ICD RNA and 0.5ng of either GFP or β gal RNA as an injection tracer. Transverse 18 μ m sections cut by cryosectioning through embryos at NF stage 15-40. Anterior and posterior CNS sections are shown oriented dorsal on top. N = 2 ISH and 5 embryos sectioned for each. Abbreviations: e, eye; fb, forebrain; hb, hindbrain; mb, midbrain; np, neural plate; olf, olfactory; ot, otic vesicle. All embryos injected on the left side. Scale bar represents 150 μ m.

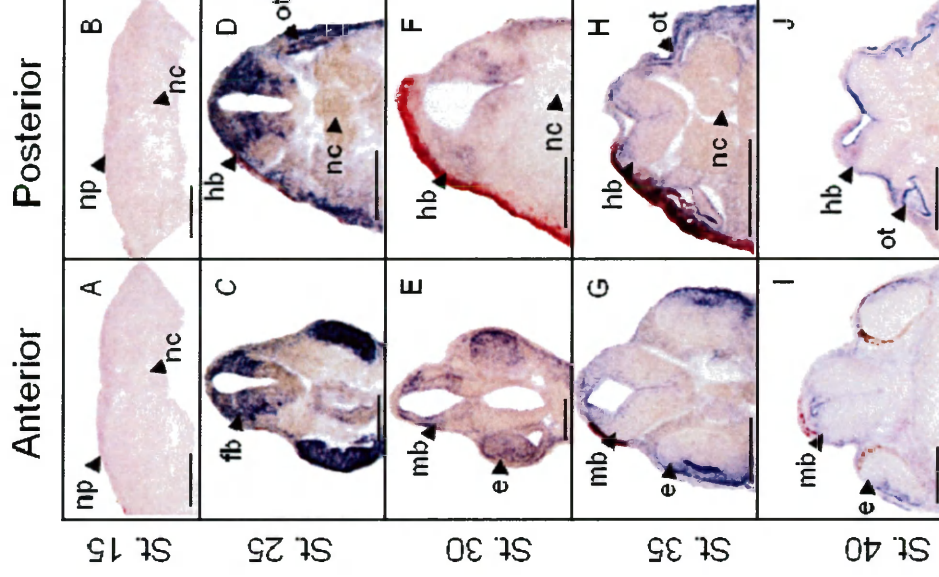


Figure 7. PCNA Expression in DBM injected embryos
 Histological analysis of PCNA expression (purple staining) detected by *in situ* hybridization in embryos unilaterally injected with 1.5 ng xSu(H) DBM RNA and 0.5ng of either GFP or β gal RNA as an injection tracer. Transverse 18 μ m sections cut by cryosectioning through embryos at NF stage 15-40. Anterior and posterior CNS sections are shown oriented dorsal on top. N = 2 ISH and 5 embryos sectioned for each. Abbreviations: e, eye; fb, forebrain; hb, hindbrain; mb, midbrain; np, neural plate; olf, olfactory; ot, otic vesicle. All embryos injected on the left side. Scale bar represents 150 μ m.

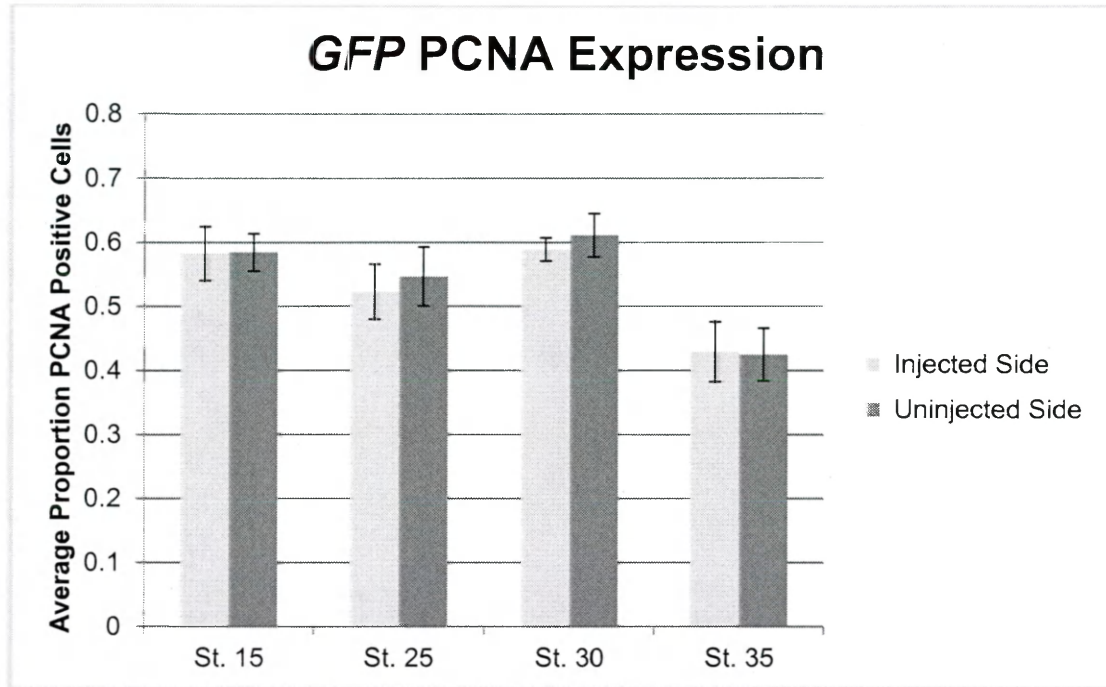


Figure 8. PCNA Cell Counts for GFP-injected embryos.

Embryos were unilaterally injected at the two-cell stage with 0.5 ng of either GFP or β -galactosidase RNA as an injection control. Embryos were assayed for expression of proliferating cell nuclear antigen (PCNA) by *in situ* hybridization and fixed at the stages on the x-axis. Transverse 18 μ m sections were taken along the anterior-posterior axis. Tissue was stained with DAPI and PCNA-positive cells were counted in the injected and control halves of the neural tissue. Bars represent the total number of positive cells in each side normalized to the total number of neural cells for that side of the embryo. Error bars represent one standard deviation.

Table 6. PCNA Cell Counts for Vehicle-Injected Controls

Stage	PCNA positive cell average- Injected Side	standard deviation	PCNA positive cell average- Uninjected Side	standard deviation	p value (n=5)
St. 15	0.583	0.084	0.585	0.0583	0.967
St. 25	0.523	0.086	0.547	0.092	0.409
St. 30	0.589	0.036	0.611	0.067	0.207
St. 35	0.429	0.093	0.425	0.082	0.713

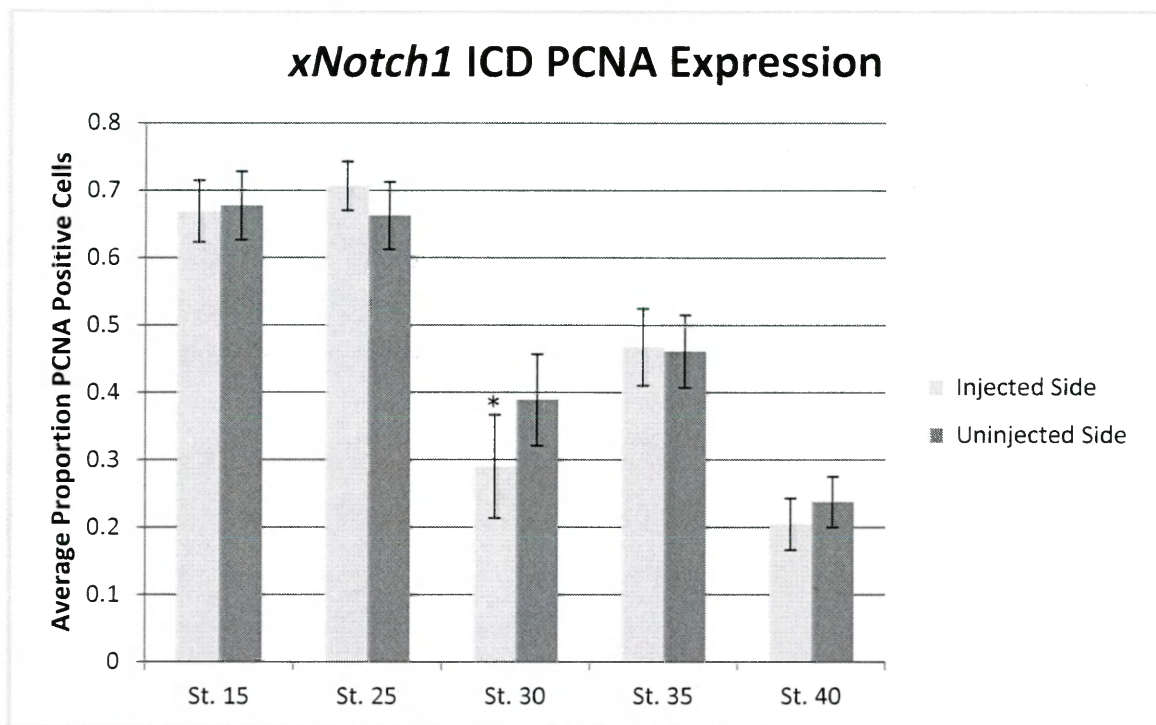


Figure 9. PCNA Cell Counts for ICD-injected embryos.

Embryos were unilaterally injected at the two-cell stage with 1.5 ng xNotch1 ICD RNA and 0.5 ng of either GFP or β -galactosidase RNA as an injection tracer. Embryos were assayed for expression of proliferating cell nuclear antigen (PCNA) by *in situ* hybridization and fixed at the stages on the x-axis. Transverse 18 μ m sections were taken along the anterior-posterior axis. Tissue was stained with DAPI and PCNA-positive cells were counted in the injected and control halves of the neural tissue. Bars represent the total number of positive cells in each side normalized to the total number of neural cells for that side of the embryo. Error bars represent one standard deviation. Asterisk indicates statistical significance ($p < 0.05$).

Table 7. PCNA Cell Counts for ICD-injected embryos.

Stage	PCNA positive cell average- Injected Side	standard deviation	PCNA positive cell average- Uninjected Side	standard deviation	p value (n=5)
St. 15	0.669	0.091	0.678	0.101	0.652
St. 25	0.707	0.073	0.663	0.099	0.300
St. 30	0.290	0.153	0.389	0.136	0.009
St. 35	0.468	0.114	0.461	0.108	0.486
St. 40	0.205	0.077	0.238	0.075	0.115

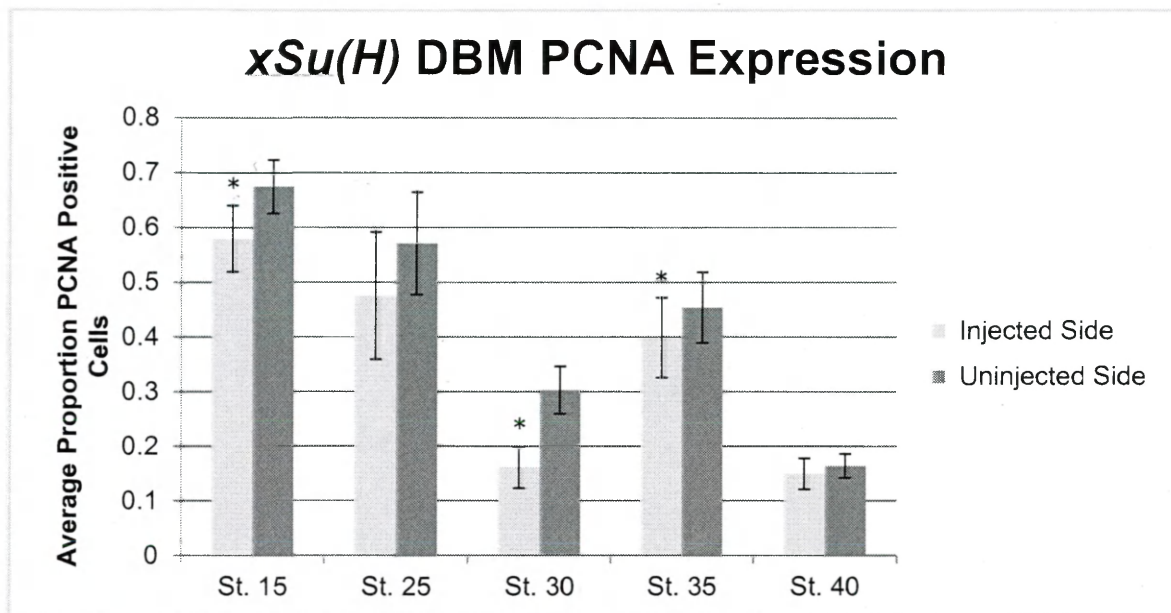


Figure 10. PCNA Cell Counts for DBM-injected embryos.

Embryos were unilaterally injected at the two-cell stage with 1.5 ng xSu(H) DBM RNA and 0.5 ng of either GFP or β -galactosidase RNA as an injection tracer. Embryos were assayed for expression of proliferating cell nuclear antigen (PCNA) by *in situ* hybridization and fixed at the stages on the x-axis. Transverse 18 μ m sections were taken along the anterior-posterior axis. Tissue was stained with DAPI and PCNA-positive cells were counted in the injected and control halves of the neural tissue. Bars represent the total number of positive cells in each side normalized to the total number of neural cells for that side of the embryo. Error bars represent one standard deviation. Asterisk indicates statistical significance ($p < 0.05$).

Table 8. PCNA Cell Counts for DBM-injected embryos.

Stage	PCNA positive cell average- Injected Side	standard deviation	PCNA positive cell average- Uninjected Side	standard deviation	p value (n=5)
St. 15	0.580	0.121	0.675	0.097	0.006
St. 25	0.476	0.233	0.572	0.187	0.309
St. 30	0.161	0.074	0.303	0.087	0.014
St. 35	0.399	0.146	0.454	0.129	0.038
St. 40	0.149	0.057	0.164	0.044	0.090

5.3 Effects of Notch Perturbation on Apoptosis

To investigate the possible role of apoptosis in the recovery from Notch perturbation, we compared the degree of apoptosis between control and perturbed sides of construct-injected embryos. The TUNEL assay allowed for the labeling of cells with nicked DNA, a characteristic sign of apoptosis. Embryos unilaterally injected with either *xNotch1 ICD* or *xSu(H) DBM* and an injection tracer were fixed at the desired stages and subjected to terminal deoxynucleotidyl transferase dUTP nicked end labeling (TUNEL) which stained positive cells dark blue. Transverse 18 μm sections taken along the anterior-posterior axis of each injected embryo were imaged and used to count individual labeled cells in the neural tissue of each side. TUNEL-positive totals were normalized to the total number of neural cells in that side to account for differences in cell population.

While there was a clear increase in apoptosis with developmental age, vehicle-injected control embryos exhibited no significant difference in the amount of apoptosis between perturbed and control sides (Fig. 11). However, embryos injected with *xNotch1 ICD* RNA displayed significantly higher levels of apoptosis on the injected side when compared to the internal control at late tailbud stage 35 ($p=0.023$) (Fig.12, Table 11). Representative images for *ICD* embryos labeled with TUNEL are shown in Figure 10. Embryos injected with *xSu(H) DBM* RNA did not demonstrate a significant difference in apoptosis between control and injected sides at any stage examined (Table 12); however, *DBM* embryos exhibited a downward trend in apoptosis rates as development

progresses (Fig. 13). Representative images of *DBM*-injected embryos labeled with TUNEL are shown at each stage in Figure 9.

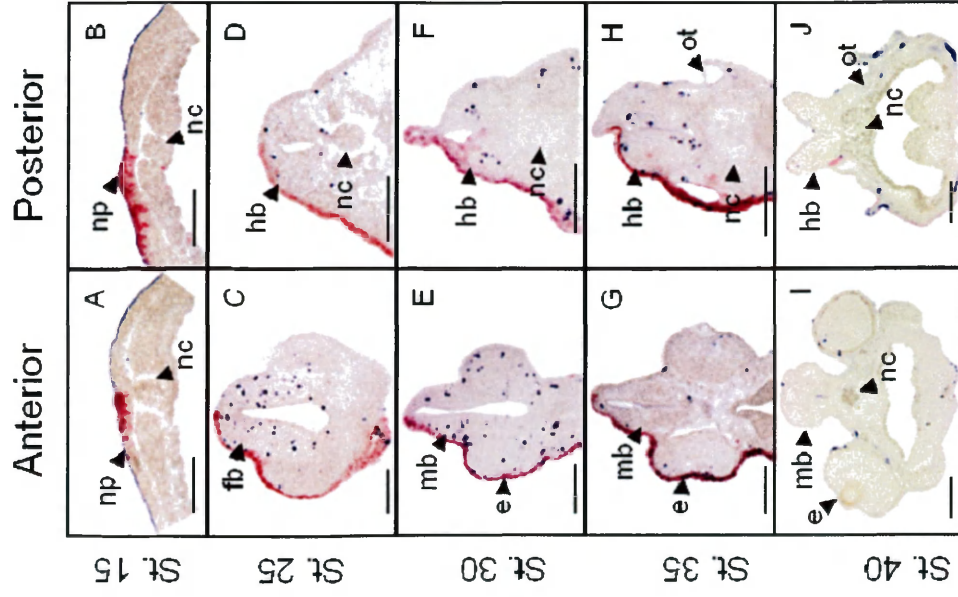


Fig. 11 TUNEL labeling in DBM-injected embryos

Histological analysis of TUNEL (blue staining) in embryos unilaterally injected with 1.5 ng *xSu(H)* DBM RNA and 0.5ng of either *GFP* or *βgal* RNA as an injection tracer. Transverse 18μm sections cut by cryosectioning through embryos at NF stage 15-40. Anterior and posterior CNS sections are shown oriented dorsal on top. N = 2 ISH and 5 embryos sectioned for each. Abbreviations: e, eye; fb, forebrain; hb, hindbrain; mb, midbrain; np, neural plate; olf, olfactory; ot, otic vesicle. All embryos injected on the left side. Scale bar represents 150 μm.

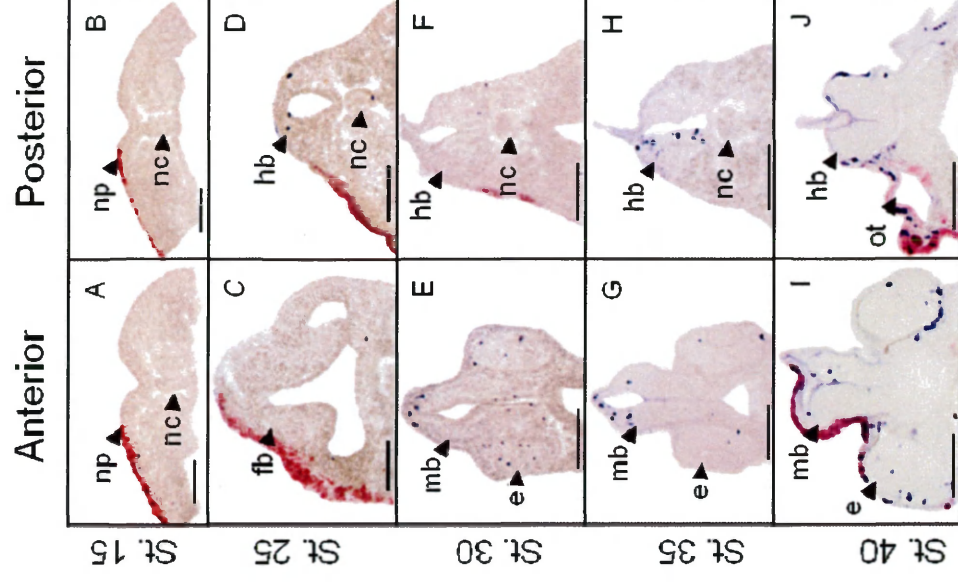


Fig. 12 TUNEL labeling in ICD-injected embryos

Histological analysis of TUNEL (blue staining) in embryos unilaterally injected with 1.5 ng *xNotch1* ICD RNA and 0.5ng of either *GFP* or *βgal* RNA as an injection tracer. Transverse 18μm sections cut by cryosectioning through embryos at NF stage 15-40. Anterior and posterior CNS sections are shown oriented dorsal on top. N = 2 ISH and 5 embryos sectioned for each. Abbreviations: e, eye; fb, forebrain; hb, hindbrain; mb, midbrain; np, neural plate; olf, olfactory; ot, otic vesicle. All embryos injected on the left side. Scale bar represents 150 μm.

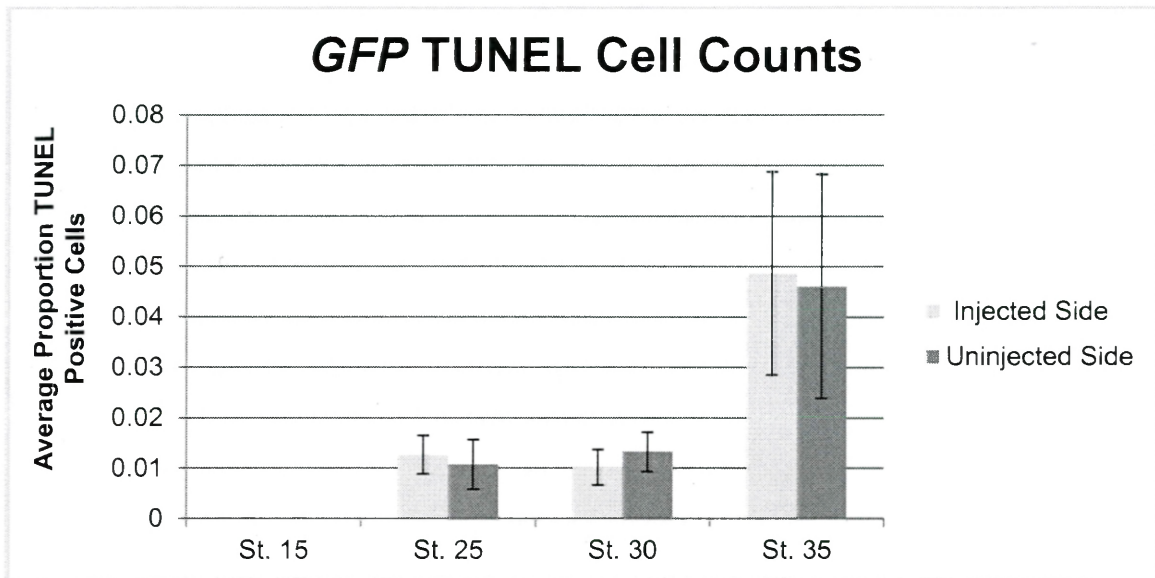


Figure 13. TUNEL Cell Counts for GFP-injected embryos.

Embryos were unilaterally injected at the two-cell stage with 0.5 ng of either GFP or β -galactosidase RNA as an injection control. Embryos were assayed for apoptotic cells using TUNEL and fixed at the stages on the x-axis. Transverse 18 μ m sections were taken along the anterior-posterior axis. Tissue was stained with DAPI and TUNEL-positive cells were counted in the injected and control halves of the neural tissue. Bars represent the total number of positive cells in each side normalized to the total number of neural cells for that side of the embryo. Error bars represent one standard deviation.

Table 9. TUNEL Cell Counts for GFP-injected embryos.

Stage	TUNEL positive cell average- Injected Side	standard deviation	TUNEL positive cell average-Injected Side	standard deviation	p value (n=5)
St. 15	6.5E-05	0.000	0.000	0.000	0.622
St. 25	0.013	0.008	0.011	0.009	0.693
St. 30	0.010	0.007	0.013	0.008	0.375
St. 35	0.049	0.040	0.046	0.044	0.416

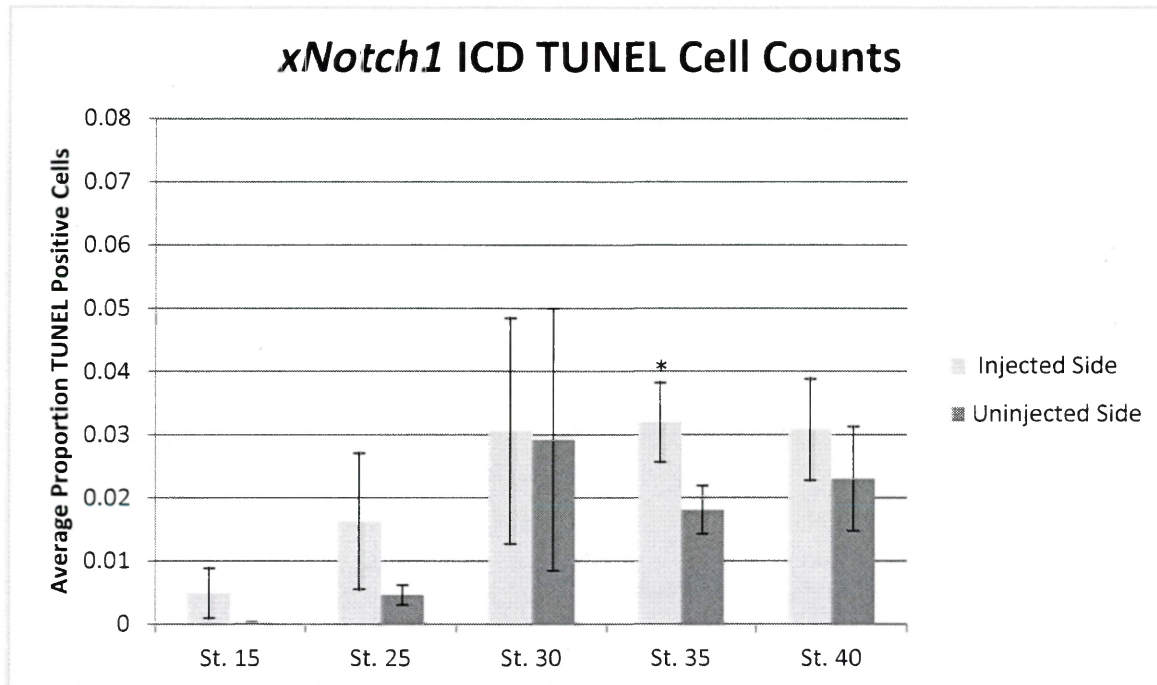


Figure 14. TUNEL Cell Counts for ICD-injected embryos.

Embryos were unilaterally injected at the two-cell stage with 1.5 ng xNotch1 ICD RNA and 0.5 ng of either GFP or β -galactosidase RNA as an injection tracer. Embryos were assayed for apoptotic cells using TUNEL and fixed at the stages on the x-axis.

Transverse 18 μ m sections were taken along the anterior-posterior axis. Tissue was stained with DAPI and TUNEL-positive cells were counted in the injected and control halves of the neural tissue. Bars represent the total number of positive cells in each side normalized to the total number of neural cells for that side of the embryo. Error bars represent one standard deviation. Asterisk indicates statistical significance ($p < 0.05$).

Table 10. TUNEL Cell Counts for ICD-injected embryos.

Stage	TUNEL positive cell average- Injected Side	standard deviation	TUNEL positive cell average-Injected Side	standard deviation	p value (n=5)
St. 15	0.005	0.008	0.000	0.000	0.253
St. 25	0.016	0.022	0.005	0.003	0.231
St. 30	0.031	0.036	0.029	0.041	0.796
St. 35	0.032	0.013	0.018	0.008	0.023
St. 40	0.031	0.016	0.023	0.017	0.236

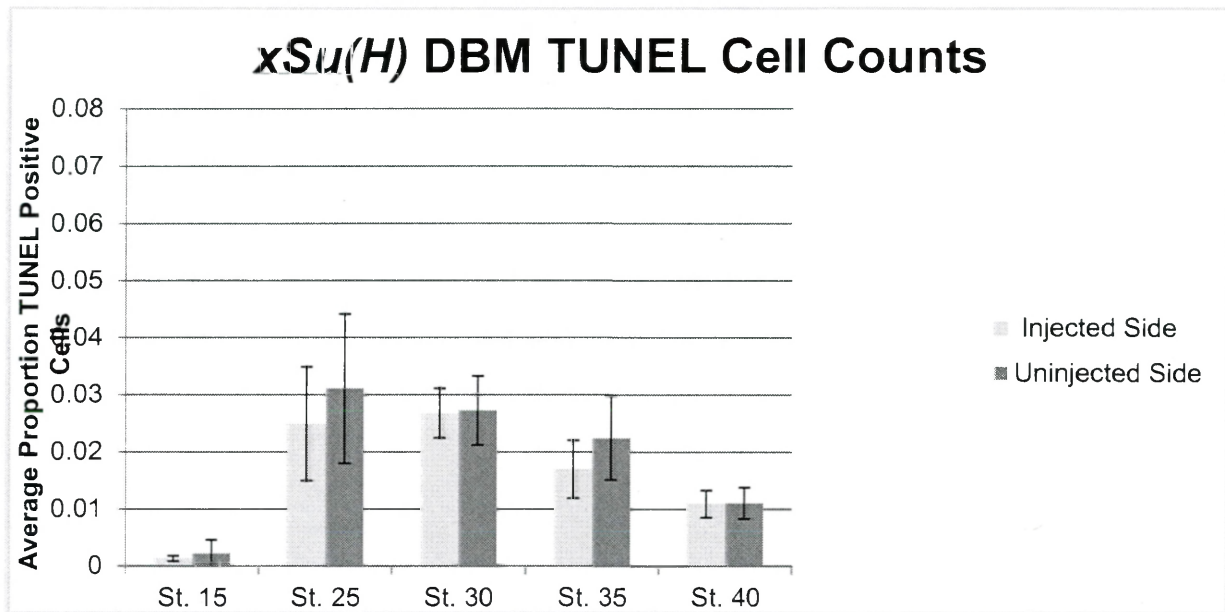


Figure 15. TUNEL Cell Counts for DBM-injected embryos.

Embryos were unilaterally injected at the two-cell stage with 1.5 ng *xSu(H)* DBM RNA and 0.5 ng of either GFP or β -galactosidase RNA as an injection tracer. Embryos were assayed for apoptotic cells using TUNEL and fixed at the stages on the x-axis. Transverse 18 μ m sections were taken along the anterior-posterior axis. Tissue was stained with DAPI and TUNEL-positive cells were counted in the injected and control halves of the neural tissue. Bars represent the total number of positive cells in each side normalized to the total number of neural cells for that side of the embryo. Error bars represent one standard deviation.

Table 11. TUNEL Cell Counts for DBM-injected embryos.

Stage	TUNEL positive cell average- Injected Side	standard deviation	TUNEL positive cell average-Injected Side	standard deviation	p value (n=5)
St. 15	0.001	0.001	0.002	0.005	0.666
St. 25	0.025	0.019	0.031	0.026	0.186
St. 30	0.027	0.009	0.027	0.012	0.948
St. 35	0.017	0.010	0.022	0.015	0.129
St. 40	0.011	0.005	0.011	0.005	0.904

5.4 Expression Profiles of Apoptosis Candidate Genes

To explore the mechanisms of apoptosis regulation involved in the compensation process, genes from several apoptosis pathways, both intrinsic and extrinsic, were chosen for study. Candidate gene expression in normal development was first profiled using whole mount *in situ* hybridization at developmental stages from neural plate (stage 15) through swimming tadpole (stage 35). Whole mount expression was analyzed and results are summarized in Table 12. Embryos assayed for candidate genes that exhibited localized expression were also transversely sectioned along the anterior-posterior axis for histological analysis of expression. Representative histological images are shown in Figures 16 - 17.

Gene	Accession #	Clone Origin	Control Expression in ISH	Developmental Stage of Expression	Documented Expression
<i>PERP</i>	NM_001092762.1	bp 112-1527	Cement gland, notochord, neural tube floor plate	tailbud, swimming tadpole	cement gland, cloaca, proctodeum
<i>casp9</i>	NM_001085566.1	bp 23-1023	CNS, eye, olfactory	swimming tadpole	brain, heart, intestine, thymus, whole organism
<i>bcl2</i>	NM_001146093.1	bp 289-811	No signal	tailbud	brain, head, pancreas, testis, whole organism
<i>casp3</i>	NM_001087756.1	bp 84-684	No signal	swimming tadpole	bone tissue, brain, central nervous system, central retina, egg, epithelium, eye, fat, body, head, heart, intestine, lens, lung, muscle, neural plate, ovary, oviduct, retina, skeletal muscle, skin, spleen, stomach, tail, upper blastopore lip, whole organism
<i>casp6</i>	NM_001087937.1	bp 770-2012	CNS	tailbud, swimming tadpole	animal cap, brain, ectoderm, egg, endomesoderm, eye, head, intestine, ovary, testis, upper blastopore lip, whole organism
<i>casp7</i>	NM_001097803.1	bp 153-1502	Lens	swimming tadpole	Keller explant, ectoderm, egg, eye, head, intestine, oocyte, ovary, oviduct, spleen, stomach, thymus, whole organism
<i>bax</i>	AF288809.1	bp 26-1241	No signal	neural plate	Keller explant, ectoderm, egg, endomesoderm, muscle, oocyte, ovary, tail, whole organism
<i>tp53</i>	NM_001088098.1	bp 957-1995	Head, pronephros	swimming tadpole	brain, head, mesoderm, notochord, otic vesicle, tail bud, ventral pronephric mesenchyme
<i>EndoG</i>	NM_001095249.1	GE, MXL1736-202784774	No signal	late tailbud	ectoderm, egg, endomesoderm, limb, lung, skin, spleen, testis, upper blastopore lip, whole organism
<i>AIFM2</i>	NM_001097928.1	GE, MXT1765-202751371	Epidermis	late tailbud	ectoderm endomesoderm head heart kidney lung spleen brain digestive animal cap

Table 12. Expression of candidate genes assayed by *in situ* hybridization in control embryos.

Protein	Role in Apoptosis	Major Regulation Mechanisms
Perp	P53-mediated Apoptosis Effector	Transcriptional regulation by p53
Caspase9	Intrinsic apoptosis initiator caspase	Proteolytic cleavage, requires apoptosome complex; inhibited by IAPs
Caspase3	Intrinsic apoptosis effector caspase	Proteolytic cleavage; inhibited by IAPs; transcriptional regulation
Caspase7	Intrinsic apoptosis effector caspase	Proteolytic cleavage; inhibited by IAPs; transcriptional regulation
Caspase6	Extrinsic apoptosis effector caspase	Proteolytic cleavage; transcriptional regulation
AIFM2	Caspase-independent apoptosis inducer; triggers chromatin condensation & DNA fragmentation	Proteolysis, release from mitochondria, transcriptional regulation
EndoG	Fragments DNA	Release from mitochondria
Bcl2	Apoptosis inhibitor, prevents outer mitochondrial membrane permeabilization	Inhibited by BH3-only proteins; transcriptional regulation
TP53	Transcriptional regulation of apoptosis genes; transcription-independent apoptosis through Bax & Bak activation	Repressed by Mdm2 and MdmX; activated by phosphorylation
Bax	Apoptosis inhibitor, permeabilizes mitochondrial outer membrane	Translocation to mitochondrial outer membrane; oligomerization, activated by BID; transcriptional regulation

Table 13. Apoptosis candidate gene functions and major modes of activation and repression.

Stage 25 Stage 35

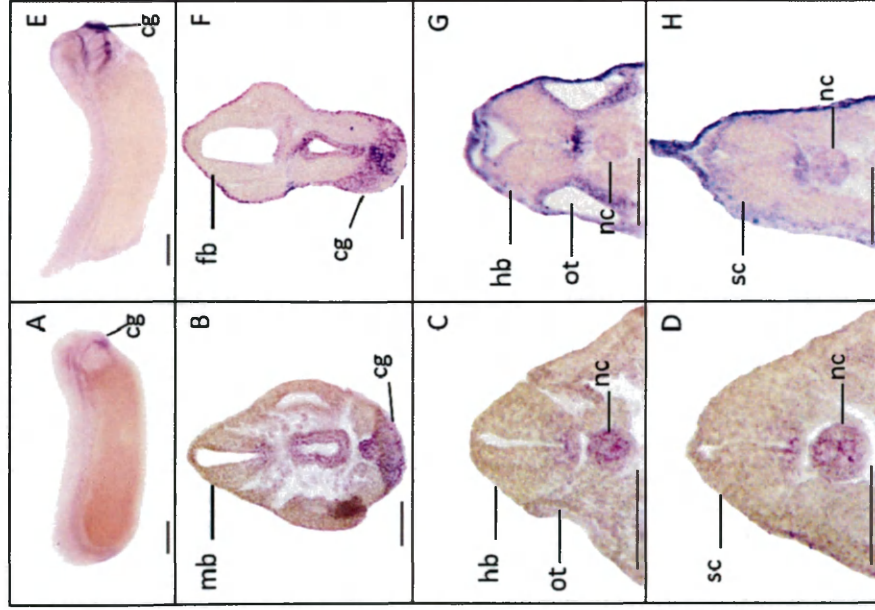


Figure 16. Expression of *Perp* in control embryos.

(a, e) Whole mount images of embryos assayed for *Perp* expression using *in situ* hybridization (purple staining). Embryos are oriented anterior to the right and dorsal to the top. (b-h) Histological analysis of *Perp* expression in transverse 18μm sections cut by cryosectioning. Sections are shown oriented dorsal on top. (b) stage 25 midbrain; (c) stage 25 hindbrain; (d) stage 35 spinal cord; (f) stage 35 forebrain; (g) stage 35 hindbrain; (h) stage 35 spinal cord. Abbreviations: fb, forebrain; hb, hindbrain; mb, midbrain; nc, notochord; ot, otic vesicle. Scale bar represents 1mm (a,e) and 150 μm (b-h).

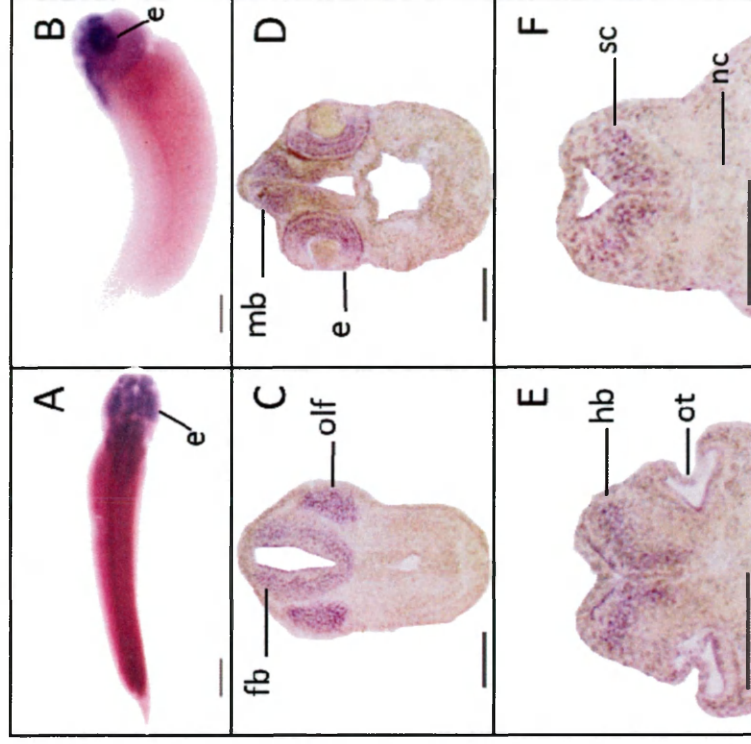


Figure 17. Expression of *Caspase9* in control embryos.

Whole mount images of embryos at stage 35 assayed for *Casp9* expression using *in situ* hybridization (purple staining). Dorsal view (a) and lateral view with dorsal to the top (b) are oriented with anterior to the right. (c-f) Histological analysis of *Casp9* expression in transverse 18μm sections cut by cryosectioning. Sections are shown oriented dorsal on top. (c) forebrain; (d) midbrain; (e) hindbrain; (f) spinal cord. Abbreviations: e, eye; fb, forebrain; hb, hindbrain; mb, midbrain; nc, notochord; olf, olfactory; ot, otic vesicle. Scale bar represents 1mm (a,b) and 150 μm (c-f).

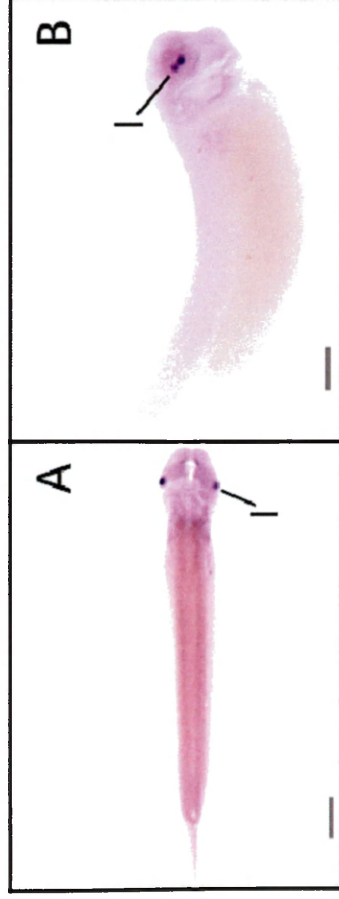


Figure 18. Expression of *Caspase7* in control embryos.

Whole mount images of embryos at stage 35 assayed for *Casp7* expression using *in situ* hybridization (purple staining). Embryos are oriented anterior to the right. Dorsal view (a) and lateral view with dorsal to the top (b). Abbreviation: l, lens. Scalebar represents 1mm.



Figure 19. Expression of *aifm2* in control embryos.

Whole mount images of embryos at stage 35 assayed for *aifm2* expression using *in situ* hybridization (purple staining). Embryo oriented anterior to the right and dorsal to the top. Abbreviations: e, eye; cg, cement gland. Scalebar represents 1mm.

5.5 Expression of Candidate Genes Following Notch Perturbation

In order to evaluate the involvement of selected apoptosis pathways in the compensatory response, candidate gene spatiotemporal expression was evaluated at a range of developmental stages in unilaterally perturbed embryos. Embryos were unilaterally injected as previously mentioned and fixed at neural plate (stage 15), tailbud (stage 25), and swimming tadpole (stage 35) stages. Fixed embryos were probed for candidate gene expression using whole mount *in situ* hybridization. Transverse histological sections were taken and used to evaluate differential candidate gene expression in the central nervous system over the compensatory time course.

Of the candidate genes analyzed, only *caspase9* and *perp* exhibited neural expression in injected embryos. Notably, *caspase9* appears to be downregulated in the injected neural tissue of *xNotch1 ICD*-injected embryos (Fig. 20, a-d; Table 13) and of *xSu(H) DBM*-injected embryos (Fig. 20, e-h) at swimming tadpole stage (stage 35). The p53-dependent apoptosis effector *Perp* displayed mild expression in the notochord and floor plate of hindbrain and anterior spinal cord at tailbud (stage 25) and swimming tadpole (stage 35) stages, though differential expression was indistinguishable.

Injection Construct	Differential Expression Pattern
<i>xNotch1 ICD</i>	Downregulated on injected side (n=3 of 5 embryos)
<i>xSu(H) DBM</i>	Downregulated on injected side (n=2 of 3 embryos)
Injection Control	Equal expression on both sides (n=2 of 2 embryos)

Table 14. Differential expression of *caspase9* in Notch-perturbed embryos (ISH n=2 for each injection condition)

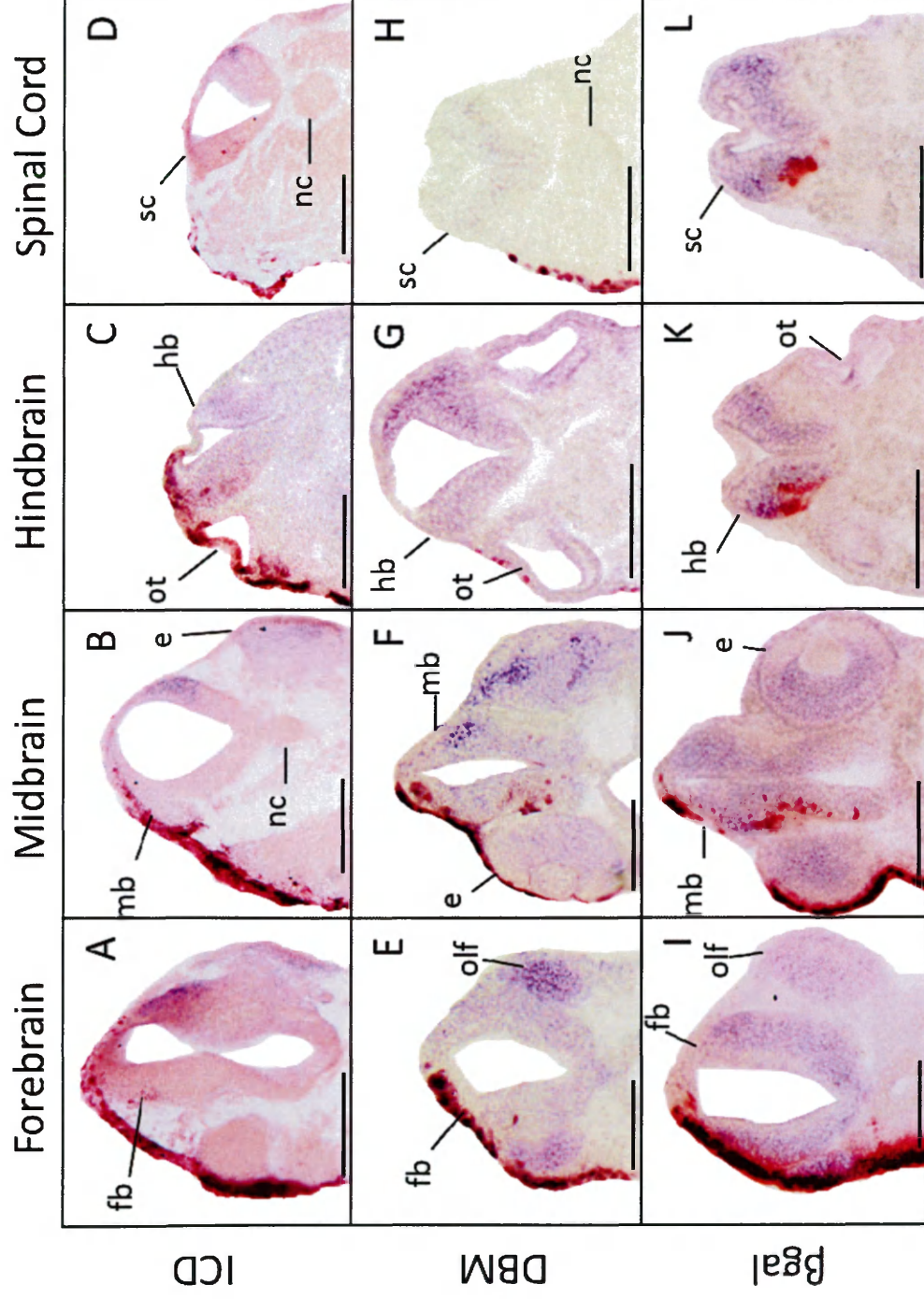


Figure 20. Expression of Caspase9 in Notch-perturbed embryos

Histological analysis of *Casp9* expression (purple staining) detected by *in situ* hybridization in embryos unilaterally injected with 1.5 ng *xSu(H)* DBM RNA and 0.5ng of β gal RNA as an injection tracer (red staining). Transverse 18 μ m sections cut by cryosectioning though embryos at stage 35. CNS sections of the regions indicated are shown oriented dorsal on top. Abbreviations: e, eye; fb, forebrain; hb, hindbrain; mb, midbrain; olf, olfactory; ot, otic vesicle; sc, spinal cord. All embryos injected on the left side. Scale bar represents 150 μ m.

Chapter 6: Discussion

The purpose of this study was to investigate the role of cellular proliferation and apoptosis in the compensatory response from early Notch signaling perturbation in neural development. We found that early unilateral Notch signaling upregulation results in increased cell number within perturbed neural tissue relative to internal controls that, rather than amplifying over time, equalizes over the course of primary neurogenesis. Cell death and proliferation appear to play key roles in this normalization, as the rates of both processes differ between sides at key points in the response process. These results implicate the regulation of cell death and division as major strategies for developmental plasticity in the nervous system.

6.1 Cell Counting Experiments

The first step in investigating apoptosis and the cell cycle as mechanisms of compensatory regulation was to examine whether the response process involved changes in cell number. Embryos with upregulated Notch signaling displayed a consistently significant increase in the average number of neural cells (normalized to the number of histological sections) from neural plate (stage 15) through swimming tadpole (stage 35) stages compared to the internal control. Cell numbers in the injected tissue of *ICD*-injected embryos were also significantly increased when compared to the injected tissue of injection control embryos at stages 15 and 30. These results are consistent with our prediction that *ICD* overexpression would increase neural cell number through the expansion of a proliferative progenitor population. It has been established that Notch

pathway activation results in the inhibition of neuronal differentiation genes and the maintenance of the proliferative progenitor state (Kageyama et al., 2009). It can be expected that embryos with increased Notch signaling will maintain a larger pool of self-renewing progenitor cells (Aujla et al., 2013) and thus exhibit increased cell numbers within the neural tube, resulting in more cells per section.

Embryos with attenuated Notch signaling display no significant difference in neural cells per section between control and injected sides at any stage. Although increased neuronal differentiation is expected with reduced Notch signaling, this may not necessarily result in an increase in gross cell number within the boundaries of neural tissue. The study by Chitnis et al. (1995) induced a neurogenic phenotype similar to those observed in *xSuh(H) DBM* embryos with a truncated form of *xDelta1* which was repeatable in the presence of cell cycle inhibitors hydroxyurea and aphidicolin (HUA). This emphasizes that an increase in commitment to the neuronal fate is not dependent on or accompanied by a concomitant increase in cell division. Moreover, a study in mammalian neurogenesis showed that Notch signaling inhibition in the hypothalamus of transgenic mice results in a reduced progenitor cell population along with the expected increase in neuronal number. In this investigation, conditional knockout of the mammalian Su(H) homolog, Rbpjk, in the proliferative region giving rise to the hypothalamus arcuate nucleus resulted in fewer progenitors marked by Sox2 expression compared to control embryos (Aujla et al., 2013). We therefore propose that, while there is no change in total cells per section between injected and control sides, there is

a reduced proportion of progenitors in *DBM*-injected tissue as a result of increased rates of progenitor differentiation into neurons.

Though our results seem contrary to reports of neural tissue expansion upon inhibition of Notch signaling in *Drosophila* and mice (Lieber et al., 1993; Aujla et al., 2013) these studies have not counted neural cell number and may reflect other changing qualities of perturbed neural tissue. During our cell number quantification we noted loose, disorganized brain tissue in *DBM* embryos (See Appendix Fig. 1). A study by Hatakeyama et al. (2004) showed that loss of the Notch target genes *Hes1* and *Hes5* in mice resulted in severely disorganized neural tissue E10.5 similar to our observations. In these mice, scanning electron micrographs showed that radial glia endfeet normally form the smooth boundary of the neural tube inner wall. The loss of radial glia in *Hes1,5* double mutants resulted in boundary disruption and cell spillage into the neural tube lumen. It may be possible that the effects of Notch signaling inhibition adversely affects cellular compaction, thus generating the hypertrophic phenotype observed by others without actually increasing cell number.

Furthermore, uninjected neural tissue in *ICD* and *DBM* embryos did not significantly differ in cell number from the control tissue of injection controls at any stage. This indicates that initial unilateral Notch perturbation does not affect tissue across the midline and that the control tissue does not regulate cell number as part of the response process.

Our next objective was to determine the involvement of apoptosis and cell division in the responsive change in neural cell population size. Following a consistent

overabundance of cells, *ICD* embryos show a significant decrease in proliferation at stage 30 followed by an increase in apoptosis at stage 35 in the injected side when compared to the internal control. This is consistent with our hypothesis that both a decreased rate of progenitor proliferation and an increase in progenitor death could be plausible mechanisms for reducing an overabundance of neural progenitors induced by Notch upregulation. Indeed, the subsequent equilibration of total cells per section between sides at stage 40 suggests that increased rates of apoptosis and decreased rates of proliferation in the preceding stages were effective in restoring population balance to an extent.

The outcomes of the apoptosis and proliferation studies in *DBM* embryos do not support our initial predictions of neuronal apoptosis and progenitor division; nonetheless, they provide insight into the embryonic mechanisms of response to disrupted population balance. Decreased levels of proliferation in *DBM*-injected embryos possibly reflect a lack of proliferative progenitor cells, an established consequence of increased differentiation induced by suppressed lateral inhibition (Aujla et al., 2013). The absence of compelling data in support of neuronal death in neurogenic *DBM* embryos suggests that altered rates of post-primary neuronal differentiation may be a mechanism behind the *xNBT* expression normalization seen in McDonough's preliminary findings.

Previous research has described a second wave of neuronal differentiation occurring after a quiescent phase that follows primary neurogenesis. Although there is no clear consensus on the timing of secondary neurogenesis in the literature, it is

loosely described as occurring during larval stages (Schlosser et al., 2002). Although the role of Notch signaling as a fate switch in this system is not well defined, a similar mechanism of lateral fate inhibition is presumed to govern later differentiation patterns, especially considering the persistent expression of Notch pathway elements observed during secondary neurogenesis (Wulliman et al., 2005). We propose that altered rates of neuronal differentiation in a second wave of neurogenesis may compensate for the overabundance of neurons induced by Notch signaling attenuation. If Notch signaling promotes lateral fate inhibition in later waves of neurogenesis as in the primary system, newly differentiated neurons may be intrinsically limited in their maximum cell density. Considering the effects of differentiation timing on neuronal phenotype it may be especially interesting to investigate the effects of compensation on the proportion of later-born neuronal subtypes (Guillemot, 2007).

6.2 Candidate Gene Expression Study

While the results of the TUNEL assays clearly suggest a role of apoptosis in mitigating the effects of early Notch perturbation, the candidate gene expression patterns are not consistent with this analysis. Decreased expression exhibited by *caspase9* in the injected sides of both *ICD* and *DBM* embryos does not support intrinsic cell death as a mechanism of the increased apoptosis seen in *ICD* embryos at stage 35. This effector caspase is continuously expressed and present as a zymogen in healthy cells and is activated through proteolytic cleavage in response to intrinsic apoptosis activation pathways (Twiddy & Cain, 2007). Furthermore, *caspase9* is a target of

transcriptional regulation of intrinsic apoptosis (Tsujimoto et al., 2005) and transcriptional upregulation has been shown to precede the initiation of cell death (Huang, 2005). Our expression results do not show evidence for the responsive initiation of intrinsic apoptosis in Notch-perturbed tissue; however, some intrinsic pathway repression is indicated. This may be a protective mechanism to prevent the death of neurons in the face of perturbation. A higher sample size is needed to confirm this phenotype. It may also be informative to investigate the expression of *caspase8*, an initiator caspase of extrinsic cell death pathways, in Notch-perturbed embryos.

Though transcription of certain core components such as *caspase9* is shown to be upregulated prior to apoptosis, many of the proteins involved in apoptotic cascades are regulated significantly by post-translational modifications and protein-protein interactions. While many of the apoptotic effector candidate genes did not show evidence of differential regulation in response to Notch perturbation, this could indicate either a post-transcriptional regulation or a lack of apoptotic activation pathway involvement (See Table 13). Finer variances in transcriptional activation may also be beyond the sensitivity of analysis by *in situ* hybridization; an ongoing RNAseq study may prove to be more revealing in this aspect.

6.3 Future Directions

The results of the proliferation and apoptosis studies in *ICD*-injected embryos suggest that *neural progenitors* are the target population for compensatory regulation. While our analysis implicates progenitor cell death as a compensatory mechanism in Notch-upregulated embryos, an important future direction is to confirm the identity of the cells undergoing apoptosis. A cell counting experiment similar to those performed in this study could be utilized to determine the predominant population undergoing significantly differential cell death. Embryos assayed by *in situ* hybridization for *xNBT* or *Sox2* to mark neurons and neural progenitors, respectively, will be subjected to TUNEL, allowing for the determination of apoptotic cell identity.

Our results also indicate that progenitor proliferation rates are decreased in Notch-upregulated embryos. Given the established correlation between progenitor subtype and position along anterior-posterior and dorsal-ventral axes (reviewed by Guillemot, 2007) it would be interesting to identify the specific progenitor subpopulations under regulation. This could be done through analysis of PCNA-positive cells in embryos assayed for expression of brain regional markers including *Otx-2* (forebrain), *En-2* (midbrain), *Krox-20* (hindbrain), and *XIHbox-6* (spinal cord).

In line with this hypothesis, regional evaluation of existing cell count data may reveal regions of the CNS that are differentially involved in the plastic response. During the course of our cell count studies we noted differences in PCNA and TUNEL signal abundance in varying regions of the brain along the anterior-posterior axis. As we subdivide the counts for each embryo into macroscopic neural regions (forebrain,

midbrain, hindbrain, and spinal cord) we may be able to discern regional differences in responsive regulation.

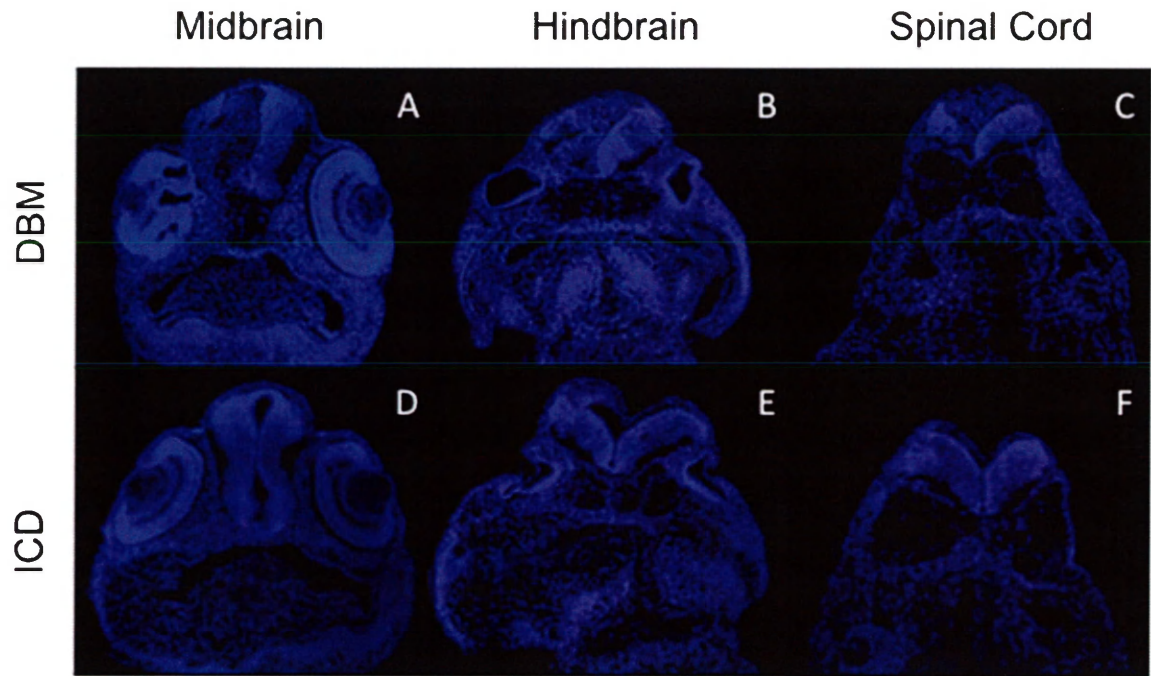
A possible step to further evaluate the relationship between early Notch misregulation and the effects on gross neural tissue size is to investigate changing proportions of progenitor, glial, and neuronal cells. Obtaining cell counts for neuronal, glial, and progenitor populations over time will reveal the dynamic response of each population and provide insight into the targets of compensation as well as supplement the earlier findings of Notch perturbation in *Xenopus* neurodevelopment. Although it has been demonstrated that Notch attenuation increases neuron cell number and density, the corresponding effects on the progenitor population have not been quantified in *Xenopus*. Additionally, while it is known that gliogenesis normally follows neurogenesis in the *Xenopus* retina, the onset of glial production in the CNS is not well defined and may explain the disorganization of neural tissue in later stage *DBM* embryos (Mochizuki et al., 2009; Hatakeyama et al., 2004). Analysis of cell type population dynamics may be achieved using the same experimental design as previously described to concurrently compare cell counts in histological sections of embryos assayed for *xNBT*, *Sox2*, and the glial marker *vimentin* (Kiyota et al., 2007).

Additionally, we may pursue the alternative hypothesis that the response from Notch perturbation involves changing rates of progenitor differentiation in addition to influencing cell death and birth rates. Double *in situ* hybridization assays probing for expression of *xNBT* and *Sox2* will reveal cells in the process of differentiation. Altered rates of differentiation in later stages of neurogenesis may account for the recovery

from neuronal deficit and overabundance seen in preliminary studies (Mcdonough, unpublished). We predict that if differentiation is employed as a mechanism of plasticity, we will observe higher levels of *xNBT* and *Sox2* coexpression over time in *ICD* injected tissue compared to vehicle-injected controls. Conversely, we predict that *DBM*-injected embryos will display lower levels of coexpression at later stages in the injected tissue compared to controls.

Finally, analysis of cell cycle regulatory gene expression may help elucidate the molecular targets of proliferation regulation in the response from early Notch perturbation. Following a similar candidate gene approach, the involvement of cell cycle genes implicated in RNAseq results will be confirmed through *in situ* hybridization. Considering that many apoptosis and cell cycle factors are post-translationally regulated (McIlwain et al., 2013; Kruse & Gu, 2009; van Delft et al., 2006; Lamb & Hardwick, 2013; Sevrioukova, 2011; Ola et al, 2011; Reidl & Shi, 2004), immunohistochemical analysis of relative activated protein levels for both cell cycle and apoptosis candidates in unilaterally perturbed embryos will be an important step in understanding the pathways involved in compensation. Functional studies will also help to establish the role of each candidate gene in the response process. Analysis of the degree and duration of compensation following temporally controlled knockdown or overexpression of candidates after the start of neurogenesis in unilaterally Notch-perturbed embryos will indicate the degree of involvement of each factor. From these results we may elaborate on involved mechanisms by investigating related pathway components for functionally implicated candidates.

Appendix



Supplemental Figure 1. Injected tissue morphology of DBM and ICD injected embryos. (a-c) Histological 18 μ m sections of stage 40 embryos unilaterally injected with *DBM* RNA and β -gal RNA as tracer at the two-cell stage. Note disorganized/loose cells in the left half of the neural tube. (d-f) Histological 18 μ m sections of stage 40 embryos unilaterally injected with *ICD* RNA and β -gal RNA as tracer at the two-cell stage. Note expanded tissue in the left half of the neural tube. Sections stained with DAPI (blue) to visualize individual cells. Sections oriented dorsal to the top. All embryos injected on the left side.

Stage	ICD Cells per Section	GFP Cells per Section	p value
st 15	60.9	53.5	0.498
st 25	43.6	51.6	0.133
st 30	83.3	74.8	0.329
st 35	48.4	43.7	0.491

Supplemental Table 1. Uninjected tissue comparison of Neural cells per section in ICD and vehicle-injected embryos.

Stage	DBM Cells per Section	GFP Cells per Section	p value
st 15	59.9	53.5	0.598
st 25	48.9	51.6	0.532
st 30	77.1	74.8	0.775
st 35	50.9	43.7	0.152

Supplemental Table 2. Uninjected tissue comparison of Neural cells per section in DBM and vehicle-injected embryos.

Stage	ICD Proportion PCNA Cells	GFP Proportion PCNA Cells	p value
st 15	0.677	0.584	0.122
st 25	0.662	0.546	0.093
st 30	0.389	0.611	0.017
st 35	0.461	0.425	0.568

Supplemental Table 3. Uninjected tissue comparison of Neural PCNA-positive cell proportion in ICD and vehicle-injected embryos.

Stage	DBM Proportion PCNA Cells	GFP Proportion PCNA Cells	p value
st 15	0.675	0.584	0.120
st 25	0.571	0.546	0.796
st 30	0.302	0.611	0.0
st 35	0.453	0.425	0.689

Supplemental Table 4. Uninjected tissue comparison of Neural PCNA-positive cell proportion in DBM and vehicle-injected embryos.

Stage	ICD Proportion TUNEL Cells	GFP Proportion TUNEL Cells	p value
st 15	0.0	0.0	0.477
st 25	0.004	0.011	0.241
st 30	0.029	0.013	0.442
st 35	0.018	0.046	0.233

Supplemental Table 5. Uninjected tissue comparison of Neural TUNEL-positive cell proportion in ICD and vehicle-injected embryos.

Stage	DBM Proportion TUNEL Cells	GFP Proportion TUNEL Cells	p value
st 15	0.002	0.0	0.377
st 25	0.031	0.011	0.164
st 30	0.027	0.013	0.066
st 35	0.022	0.046	0.309

Supplemental Table 6. Uninjected tissue comparison of Neural TUNEL-positive cell proportion in DBM and vehicle-injected embryos.

Stage	ICD Cells per Section	GFP Cells per Section	p value
st 15	85.9	56.8	0.017
st 25	64.2	51.6	0.274
st 30	109.0	71.2	0.005
st 35	57.6	42.0	0.094

Supplemental Table 7. Injected tissue comparison of Neural cells per section in ICD and vehicle-injected embryos.

Stage	GFP Cells per Section	GFP Cells per Section	p value
st 15	50.8	56.8	0.597
st 25	50.6	51.6	0.817
st 30	79.3	71.2	0.392
st 35	48.1	42.0	0.229

Supplemental Table 8. Injected tissue comparison of Neural cells per section in DBM and vehicle-injected embryos.

Stage	ICD Proportion PCNA Cells	GFP Proportion PCNA Cells	p value
st 15	0.669	0.582	0.159
st 25	0.706	0.522	0.006
st 30	0.290	0.588	0.0104
st 35	0.467	0.429	0.579

Supplemental Table 9. Injected tissue comparison of Neural PCNA-positive cell proportion in ICD and vehicle-injected embryos.

Stage	DBM Proportion PCNA Cells	GFP Proportion PCNA Cells	p value
st 15	0.580	0.582	0.229
st 25	0.475	0.522	0.689
st 30	0.160	0.588	3.08E-05
st 35	0.398	0.429	0.704

Supplemental Table 10. Injected tissue comparison of Neural PCNA-positive cell proportion in DBM and vehicle-injected embryos.

Stage	ICD Proportion TUNEL Cells	GFP Proportion TUNEL Cells	p value
st 15	0.0049	6.49E-05	0.245
st 25	0.0163	0.0127	0.740
st 30	0.0305	0.0102	0.274
st 35	0.0320	0.0487	0.418

Supplemental Table 11. Injected tissue comparison of Neural TUNEL-positive cell proportion in ICD and vehicle-injected embryos.

Stage	DBM Proportion TUNEL Cells	GFP Proportion TUNEL Cells	p value
st 15	0.0013	6.49E-05	0.043
st 25	0.0249	0.0127	0.255
st 30	0.0268	0.0102	0.011
st 35	0.0170	0.0487	0.155

Supplemental Table 12. Injected tissue comparison of Neural TUNEL-positive cell proportion in DBM and vehicle-injected embryos.

Neural Cells per Section	p value	Tukey HSD Test
ICD Injected	0.0018	25 vs 30 $P < .01$; 30 vs 35 $P < .01$
ICD Uninjected	$< .0001$	25 vs 30 $P < .01$; 25 vs 40 $P < .05$; 30 vs 35 $P < .01$; 35 vs 40 $P < .05$
DBM Injected	$< .0001$	15 vs 30 $P < .05$; 15 vs 40 $P < .01$; 25 vs 30 $P < .05$; 25 vs 40 $P < .01$; 30 vs 35 $P < .01$; 35 vs 40 $P < .01$
DBM Uninjected	$< .0001$	15 vs 40 $P < .01$; 25 vs 30 $P < .01$; 25 vs 40 $P < .01$; 30 vs 35 $P < .05$; 35 vs 40 $P < .01$
GFP Injected	0.0043	30 vs 35 $P < .01$
GFP Uninjected	0.0035	St 25 vs St 35 $p < 0.05$; St 30 vs St 35 $p < 0.01$

Supplemental Table 13. Comparison of average neural cells per section across all stages

Proportion of PCNA (+) Cells	p value	Tukey HSD Test
ICD Injected	$< .0001$	15 vs 30 $P < .01$; 15 vs 35 $p < .05$; 15 vs 40 $p < .01$; 25 vs 30 $p < .01$; 25 vs 35 $p < .05$; 25 vs 40 $p < .01$; 35 vs 40 $p < .01$
ICD Uninjected	$< .0001$	15 vs 30 $P < .01$; 15 vs 35 $p < .05$; 15 vs 40 $p < .01$; 25 vs 30 $p < .01$; 25 vs 35 $p < .05$; 25 vs 40 $p < .01$; 35 vs 40 $p < .05$
DBM Injected	0.0002	15 vs 30 $P < .01$; 15 vs 40 $P < .01$; 25 vs 30 $P < .05$; 25 vs 40 $P < .05$
DBM Uninjected	$< .0001$	15 vs 30 $P < .01$; 15 vs 40 $P < .01$; 25 vs 30 $P < .05$; 25 vs 40 $P < .01$; 35 vs 40 $P < .01$
GFP Injected	0.0188	15 vs 35 $P < .05$; 30 vs 35 $P < .05$
GFP Uninjected	0.0069	15 vs 35 $P < .05$; 30 vs 35 $P < .01$

Supplemental Table 14. Comparison of average proportion of PCNA-positive cells across all stages

Proportion of TUNEL (+) Cells	p value	Tukey HSD Test
ICD Injected	0.2107	N/A
ICD Uninjected	0.1627	N/A
DBM Injected	0.0088	15 vs 25 P<.05; 15 vs 30 P<.05
DBM Uninjected	0.0330	No comparison significant
GFP Injected	0.0106	15 vs 35 P<.05
GFP Uninjected	0.0339	15 vs 35 P<.05

Supplemental Table 15. Comparison of average proportion of TUNEL-positive cells across all stages

Bibliography

- Adams, J., & Cory, S. (2007). The bcl-2 apoptotic switch in cancer development and therapy. *Oncogene*, 26(9), 1324-1337.
- Andersson, E. R., Sandberg, R., & Lendahl, U. (2011). Notch signaling: Simplicity in design, versatility in function. *Development (Cambridge, England)*, 138(17), 3593-3612. doi:10.1242/dev.063610 [doi]
- Artavanis-Tsakonas, S., Matsuno, K., & Fortini, M. E. (1995). Notch signaling. *Science (New York, N.Y.)*, 268(5208), 225-232.
- Aruga, J., & Mikoshiba, K. (2011). Role of BMP, FGF, calcium signaling, and zic proteins in vertebrate neuroectodermal differentiation. *Neurochemical Research*, 36(7), 1286-1292.
- Arya, R., & White, K. (2015). Cell death in development: Signaling pathways and core mechanisms. *Seminars in Cell & Developmental Biology*, , 39 12-19.
- Aujla, P. K., Naratadam, G. T., Xu, L., & Raetzman, L. T. (2013). Notch/Rbpjkappa signaling regulates progenitor maintenance and differentiation of hypothalamic arcuate neurons. *Development (Cambridge, England)*, 140(17), 3511-3521. doi:10.1242/dev.098681 [doi]
- Bailey, A. M., & Posakony, J. W. (1995). Suppressor of hairless directly activates transcription of enhancer of split complex genes in response to notch receptor activity. *Genes & Development*, 9(21), 2609-2622.
- Batut, J., Vandel, L., Leclerc, C., Daguzan, C., Moreau, M., & Neant, I. (2005). The Ca²⁺-induced methyltransferase xPRMT1b controls neural fate in amphibian embryo. *Proceedings of the National Academy of Sciences of the United States of America*, 102(42), 15128-15133. doi:0502483102 [pii]
- Bingham, S., Chaudhari, S., Vanderlaan, G., Itoh, M., Chitnis, A., & Chandrasekhar, A. (2003). Neurogenic phenotype of mind bomb mutants leads to severe patterning defects in the zebrafish hindbrain. *Developmental Dynamics*, 228(3), 451-463.
- Bray, S., & Furriols, M. (2001). Notch pathway: Making sense of suppressor of hairless. *Current Biology*, 11(6), R217-R221.
- Buss, R. R., Sun, W., & Oppenheim, R. W. (2006). Adaptive roles of programmed cell death during nervous system development 1. *Annu.Rev.Neurosci.*, 29, 1-35.

- Castro, B., Barolo, S., Bailey, A. M., & Posakony, J. W. (2005). Lateral inhibition in proneural clusters: Cis-regulatory logic and default repression by suppressor of hairless. *Development (Cambridge, England)*, 132(15), 3333-3344. doi:dev.01920 [pii]
- Chalmers, A. D., Welchman, D., & Papalopulu, N. (2002). Intrinsic differences between the superficial and deep layers of the xenopus ectoderm control primary neuronal differentiation. *Developmental Cell*, 2(2), 171-182.
- Chenn, A., & Walsh, C. A. (2002). Regulation of cerebral cortical size by control of cell cycle exit in neural precursors. *Science (New York, N.Y.)*, 297(5580), 365-369. doi:10.1126/science.1074192 [doi]
- Chitnis, A., Henrique, D., Lewis, J., Ish-Horowicz, D., & Kintner, C. (1995). Primary neurogenesis in xenopus embryos regulated by a homologue of the drosophila neurogenic gene delta. *Nature*, 375(6534), 761-766. doi:10.1038/375761a0 [doi]
- Christopher, H., & Anna, P. (2012). Co-ordination of cell cycle and differentiation in the developing nervous system. *Biochemical Journal*, 444(3), 375-382.
- Christopher, H., & Anna, P. (2012). Co-ordination of cell cycle and differentiation in the developing nervous system. *Biochemical Journal*, 444(3), 375-382.
- Coffman, C. R., Skoglund, P., Harris, W. A., & Kintner, C. R. (1993). Expression of an extracellular deletion of xotch diverts cell fate in xenopus embryos. *Cell*, 73(4), 659-671.
- Courchesne, E., Pierce, K., Schumann, C. M., Redcay, E., Buckwalter, J. A., Kennedy, D. P., & Morgan, J. (2007). Mapping early brain development in autism. *Neuron*, 56(2), 399-413.
- Davies, L., Gray, D., Spiller, D., White, M. R., Damato, B., Grierson, I., & Paraoan, L. (2009). P53 apoptosis mediator PERP: Localization, function and caspase activation in uveal melanoma. *Journal of Cellular and Molecular Medicine*, 13(8b), 1995-2007.
- Davis, R. L., & Turner, D. L. (2001). Vertebrate hairy and enhancer of split related proteins: Transcriptional repressors regulating cellular differentiation and embryonic patterning. *Oncogene*, 20(58), 8342-8357. doi:10.1038/sj.onc.1205094 [doi]
- de la Pompa, J. L., Wakeham, A., Correia, K. M., Samper, E., Brown, S., Aguilera, R. J., . . . Conlon, R. A. (1997). Conservation of the notch signalling pathway in mammalian neurogenesis. *Development (Cambridge, England)*, 124(6), 1139-1148.

- del Corral, R. D., & Storey, K. G. (2001). Markers in vertebrate neurogenesis. *Nature Reviews Neuroscience*, 2(11), 835-839.
- Du, W., Xie, J. E., & Dyson, N. (1996). Ectopic expression of dE2F and dDP induces cell proliferation and death in the drosophila eye. *The EMBO Journal*, 15(14), 3684-3692.
- Fang, W., Chen, W., Jiang, L., Liu, K., Yung, W., Fu, A. K., & Ip, N. Y. (2014). Overproduction of upper-layer neurons in the neocortex leads to autism-like features in mice. *Cell Reports*, 9(5), 1635-1643.
- Fuchs, Y., & Steller, H. (2011). Programmed cell death in animal development and disease. *Cell*, 147(4), 742-758.
- Guillemot, F. (2007). Spatial and temporal specification of neural fates by transcription factor codes. *Development (Cambridge, England)*, 134(21), 3771-3780. doi:dev.006379 [pii]
- Hamburger, V. (1975). Cell death in the development of the lateral motor column of the chick embryo. *Journal of Comparative Neurology*, 160(4), 535-546.
- Hardwick, L. J., & Philpott, A. (2014). Nervous decision-making: To divide or differentiate. *Trends in Genetics*, 30(6), 254-261.
- Hatakeyama, J., Bessho, Y., Katoh, K., Ookawara, S., Fujioka, M., Guillemot, F., & Kageyama, R. (2004). Hes genes regulate size, shape and histogenesis of the nervous system by control of the timing of neural stem cell differentiation. *Development (Cambridge, England)*, 131(22), 5539-5550. doi:dev.01436 [pii]
- Helmy, I. M., & Azim, A. (2012). Efficacy of ImageJ in the assessment of apoptosis. *Diagn Pathol*, 7, 15.
- Hensey, C., & Gautier, J. (1998). Programmed cell death during *Xenopus* Development: A spatio-temporal analysis. *Developmental Biology*, 203(1), 36-48.
- Herrup, K., & Yang, Y. (2007). Cell cycle regulation in the postmitotic neuron: Oxymoron or new biology? *Nature Reviews Neuroscience*, 8(5), 368-378.
- Huang, W., Dobberfuhl, A., Filippopoulos, T., Ingelsson, M., Fileta, J. B., Poulin, N. R., & Grosskreutz, C. L. (2005). Transcriptional up-regulation and activation of initiating caspases in experimental glaucoma. *The American Journal of Pathology*, 167(3), 673-681.

- Huard, J. M., Forster, C. C., Carter, M. L., Sicinski, P., & Ross, M. E. (1999). Cerebellar histogenesis is disturbed in mice lacking cyclin D2. *Development (Cambridge, England)*, 126(9), 1927-1935.
- Iso, T., Kedes, L., & Hamamori, Y. (2003). HES and HERP families: Multiple effectors of the notch signaling pathway. *Journal of Cellular Physiology*, 194(3), 237-255.
- Jan, L. Y., & Jan, Y. N. (1982). Antibodies to horseradish peroxidase as specific neuronal markers in drosophila and in grasshopper embryos. *Proceedings of the National Academy of Sciences of the United States of America*, 79(8), 2700-2704.
- Johnston, R. J., Jr, & Desplan, C. (2010). Stochastic mechanisms of cell fate specification that yield random or robust outcomes. *Annual Review of Cell and Developmental Biology*, 26, 689-719. doi:10.1146/annurev-cellbio-100109-104113 [doi]
- Kageyama, R., Ohtsuka, T., Shimojo, H., & Imayoshi, I. (2009). Dynamic regulation of notch signaling in neural progenitor cells. *Current Opinion in Cell Biology*, 21(6), 733-740.
- Kim, H. S., Jeong, H., Lim, S., & Jung, G. (2013). Snail inhibits Notch1 intracellular domain mediated transcriptional activation via competing with MAML1. *Biochemical and Biophysical Research Communications*, 433(1), 6-10. doi:http://dx.doi.org/10.1016/j.bbrc.2013.02.079
- Kiyota, T., Kato, A., & Kato, Y. (2007). Ets-1 regulates radial glia formation during vertebrate embryogenesis. *Organogenesis*, 3(2), 93-101.
- Kruse, J., & Gu, W. (2009). Modes of p53 regulation. *Cell*, 137(4), 609-622.
- Kuida, K., Haydar, T. F., Kuan, C., Gu, Y., Taya, C., Karasuyama, H., . . . Flavell, R. A. (1998). Reduced apoptosis and cytochrome c-mediated caspase activation in mice lacking caspase 9. *Cell*, 94(3), 325-337.
- Kunisch, M., Haenlin, M., & Campos-Ortega, J. A. (1994). Lateral inhibition mediated by the drosophila neurogenic gene delta is enhanced by proneural proteins. *Proceedings of the National Academy of Sciences of the United States of America*, 91(21), 10139-10143.
- Lamb, H. M., & Hardwick, J. M. (2013). Unlatched BAX pairs for death. *Cell*, 152(3), 383-384.
- Lange, C., Huttner, W. B., & Calegari, F. (2009). Cdk4/cyclinD1 overexpression in neural stem cells shortens G1, delays neurogenesis, and promotes the generation and expansion of basal progenitors. *Cell Stem Cell*, 5(3), 320-331.

- Leclerc, C., Lee, M., Webb, S. E., Moreau, M., & Miller, A. L. (2003). Calcium transients triggered by planar signals induce the expression of ZIC3 gene during neural induction in xenopus. *Developmental Biology*, 261(2), 381-390.
- Leclerc, C., Webb, S. E., Daguzan, C., Moreau, M., & Miller, A. L. (2000). Imaging patterns of calcium transients during neural induction in xenopus laevis embryos. *Journal of Cell Science*, 113 Pt 19, 3519-3529.
- Li, Y., & Baker, N. E. (2001). Proneural enhancement by notch overcomes suppressor-of-hairless repressor function in the developing drosophila eye. *Current Biology*, 11(5), 330-338.
- Li, Q. J., Pazdera, T. M., & Minden, J. S. (1999). Drosophila embryonic pattern repair: How embryos respond to cyclin E-induced ectopic division. *Development (Cambridge, England)*, 126(10), 2299-2307.
- Lieber, T., Kidd, S., Alcamo, E., Corbin, V., & Young, M. W. (1993). Antineurogenic phenotypes induced by truncated notch proteins indicate a role in signal transduction and may point to a novel function for notch in nuclei. *Genes & Development*, 7(10), 1949-1965.
- Lubman, O. Y., Korolev, S. V., & Kopan, R. (2004). Anchoring notch genetics and biochemistry: Structural analysis of the ankyrin domain sheds light on existing data. *Molecular Cell*, 13(5), 619-626.
- Lundell, M. J., Lee, H. K., Perez, E., & Chadwell, L. (2003). The regulation of apoptosis by Numb/Notch signaling in the serotonin lineage of drosophila. *Development (Cambridge, England)*, 130(17), 4109-4121.
- Maier, D. (2006). Hairless: The ignored antagonist of the notch signalling pathway. *Hereditas*, 143(2006), 212-221.
- Marchal, L., Luxardi, G., Thome, V., & Kodjabachian, L. (2009). BMP inhibition initiates neural induction via FGF signaling and zic genes. *Proceedings of the National Academy of Sciences of the United States of America*, 106(41), 17437-17442. doi:10.1073/pnas.0906352106 [doi]
- Martynoga, B., Drechsel, D., & Guillemot, F. (2012). Molecular control of neurogenesis: A view from the mammalian cerebral cortex. *Cold Spring Harbor Perspectives in Biology*, 4(10), 10.1101/cshperspect.a008359. doi:10.1101/cshperspect.a008359 [doi]

- Mason, H. A., Rakowiecki, S. M., Gridley, T., & Fishell, G. (2006). Loss of notch activity in the developing central nervous system leads to increased cell death. *Developmental Neuroscience*, 28(1-2), 49-57. doi:90752 [pii]
- McIlwain, D. R., Berger, T., & Mak, T. W. (2013). Caspase functions in cell death and disease. *Cold Spring Harbor Perspectives in Biology*, 5(4), a008656. doi:10.1101/cshperspect.a008656 [doi]
- Mochizuki, T., Bilitou, A., Waters, C. T., Hussain, K., Zollo, M., & Ohnuma, S. (2009). Xenopus NM23-X4 regulates retinal gliogenesis through interaction with p27Xic1. *Neural Dev*, 4(1)
- Mogensen, J. (2011). Almost unlimited potentials of a limited neural plasticity. *Journal of Consciousness Studies*, 18(7-8), 13-45.
- Moreau, M., Leclerc, C., Gualandris-Parisot, L., & Duprat, A. M. (1994). Increased internal Ca²⁺ mediates neural induction in the amphibian embryo. *Proceedings of the National Academy of Sciences of the United States of America*, 91(26), 12639-12643.
- Moreau, M., Neant, I., Webb, S. E., Miller, A. L., & Leclerc, C. (2008). Calcium signalling during neural induction in xenopus laevis embryos. *Philosophical Transactions of the Royal Society of London. Series B, Biological Sciences*, 363(1495), 1371-1375. doi:10.1098/rstb.2007.2254 [doi]
- Nakagawa, O., McFadden, D. G., Nakagawa, M., Yanagisawa, H., Hu, T., Srivastava, D., & Olson, E. N. (2000). Members of the HRT family of basic helix-loop-helix proteins act as transcriptional repressors downstream of notch signaling. *Proceedings of the National Academy of Sciences of the United States of America*, 97(25), 13655-13660. doi:10.1073/pnas.250485597 [doi]
- Nonomura, K., Yamaguchi, Y., Hamachi, M., Koike, M., Uchiyama, Y., Nakazato, K., . . . Yoshida, H. (2013). Local apoptosis modulates early mammalian brain development through the elimination of morphogen-producing cells. *Developmental Cell*, 27(6), 621-634.
- Ola, M. S., Nawaz, M., & Ahsan, H. (2011). Role of bcl-2 family proteins and caspases in the regulation of apoptosis. *Molecular and Cellular Biochemistry*, 351(1-2), 41-58.
- Pai, V. P., Lemire, J. M., Pare, J. F., Lin, G., Chen, Y., & Levin, M. (2015). Endogenous gradients of resting potential instructively pattern embryonic neural tissue via notch signaling and regulation of proliferation. *The Journal of Neuroscience : The Official Journal of the Society for Neuroscience*, 35(10), 4366-4385. doi:10.1523/JNEUROSCI.1877-14.2015 [doi]

- Park, H., & Poo, M. (2013). Neurotrophin regulation of neural circuit development and function. *Nature Reviews Neuroscience*, 14(1), 7-23.
- Pauklin, S., & Vallier, L. (2013). The cell-cycle state of stem cells determines cell fate propensity. *Cell*, 155(1), 135-147.
- Peco, E., Escude, T., Agius, E., Sabado, V., Medevielle, F., Ducommun, B., & Pituello, F. (2012). The CDC25B phosphatase shortens the G2 phase of neural progenitors and promotes efficient neuron production. *Development (Cambridge, England)*, 139(6), 1095-1104. doi:10.1242/dev.068569 [doi]
- Richard-Parpaillon, L., Cosgrove, R. A., Devine, C., Vernon, A. E., & Philpott, A. (2004). G1/S phase cyclin-dependent kinase overexpression perturbs early development and delays tissue-specific differentiation in xenopus. *Development (Cambridge, England)*, 131(11), 2577-2586. doi:10.1242/dev.01121 [doi]
- Riedl, S. J., & Shi, Y. (2004). Molecular mechanisms of caspase regulation during apoptosis. *Nature Reviews / Molecular Cell Biology*, 5, 897.
- Riedl, S. J., & Shi, Y. (2004). Molecular mechanisms of caspase regulation during apoptosis. *Nature Reviews Molecular Cell Biology*, 5(11), 897-907.
- Roberts, A., Hill, N. A., & Hicks, R. (2000). Simple mechanisms organise orientation of escape swimming in embryos and hatchling tadpoles of xenopus laevis. *The Journal of Experimental Biology*, 203(Pt 12), 1869-1885.
- Schlosser, G., Koyano-Nakagawa, N., & Kintner, C. (2002). Thyroid hormone promotes neurogenesis in the xenopus spinal cord. *Developmental Dynamics*, 225(4), 485-498.
- Schroeter, E. H., Kisslinger, J. A., & Kopan, R. (1998). Notch-1 signalling requires ligand-induced proteolytic release of intracellular domain. *Nature*, 393(6683), 382-386.
- Sevrioukova, I. F. (2011). Apoptosis-inducing factor: Structure, function, and redox regulation. *Antioxidants & Redox Signaling*, 14(12), 2545-2579. doi:10.1089/ars.2010.3445 [doi]
- Sive, H. L., Grainger, R. M., & Harland, R. M. (2007). Xenopus laevis in vitro fertilization and natural mating methods. *CSH Protocols*, 2007, pdb.prot4737. doi:10.1101/pdb.prot4737 [doi]
- Speidel, D. (2010). Transcription-independent p53 apoptosis: An alternative route to death. *Trends in Cell Biology*, 20(1), 14-24.

- Taylor, M. K., Yeager, K., & Morrison, S. J. (2007). Physiological notch signaling promotes gliogenesis in the developing peripheral and central nervous systems. *Development (Cambridge, England)*, 134(13), 2435-2447. doi:dev.005520 [pii]
- Tsujimoto, K., Ono, T., Sato, M., Nishida, T., Oguma, T., & Tadakuma, T. (2005). Regulation of the expression of caspase-9 by the transcription factor activator protein-4 in glucocorticoid-induced apoptosis. *The Journal of Biological Chemistry*, 280(30), 27638-27644. doi:M501304200 [pii]
- Twiddy, D., & Cain, K. (2007). Caspase-9 cleavage, do you need it? *Biochem.J*, 405, e1-e2.
- van Delft, M. F., & Huang, D. C. (2006). How the bcl-2 family of proteins interact to regulate apoptosis. *Cell Research*, 16(2), 203-213.
- Vasiliu, D., Clamons, S., McDonough, M., Rabe, B., & Saha, M. (2015). A regression-based differential expression detection algorithm for microarray studies with ultra-low sample size. *PloS One*, 10(3), e0118198. doi:10.1371/journal.pone.0118198 [doi]
- Vernon, A. E., Devine, C., & Philpott, A. (2003). The cdk inhibitor p27Xic1 is required for differentiation of primary neurones in xenopus. *Development (Cambridge, England)*, 130(1), 85-92.
- Wettstein, D. A., Turner, D. L., & Kintner, C. (1997). The xenopus homolog of drosophila suppressor of hairless mediates notch signaling during primary neurogenesis. *Development (Cambridge, England)*, 124(3), 693-702.
- Wullimann, M. F., Rink, E., Vernier, P., & Schlosser, G. (2005). Secondary neurogenesis in the brain of the african clawed frog, xenopus laevis, as revealed by PCNA, Delta-1, Neurogenin-related-1, and NeuroD expression. *Journal of Comparative Neurology*, 489(3), 387-402.
- Yamaguchi, Y., Shinotsuka, N., Nonomura, K., Takemoto, K., Kuida, K., Yosida, H., & Miura, M. (2011). Live imaging of apoptosis in a novel transgenic mouse highlights its role in neural tube closure. *The Journal of Cell Biology*, 195(6), 1047-1060. doi:10.1083/jcb.201104057 [doi]
- Yang, X., Klein, R., Tian, X., Cheng, H., Kopan, R., & Shen, J. (2004). Notch activation induces apoptosis in neural progenitor cells through a p53-dependent pathway. *Developmental Biology*, 269(1), 81-94.